Macromolecules
Article
Cite This: Macromolecules 2019, 52, 8849−8866
pubs.acs.org/Macromolecules

Nonequilibrium Melt State of Ultra-High-Molecular-Weight Polyethylene: A Theoretical Approach on the Equilibrium Process

Laurence G. D. Hawke,* Dario Romano, and Sanjay Rastogi

Aachen-Maastricht Institute of BioBased Materials (AMIBM), Maastricht University, P.O. Box 616, 6200MD Maastricht, The Netherlands

Supporting Information

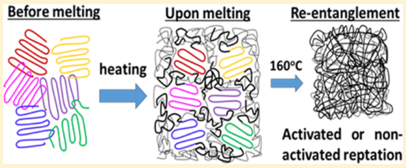

ABSTRACT: This work addresses the ability of the tube model to describe the rheological response of partially entangled, ultra-high-molecular-weight polyethylene (UHMW-PE) chains both in and out of equilibrium. It uses the tube model, in its usual form, to quantitatively describe the linear rheology of equilibrated UHMW-PE melts. Using a unique parameterization set for the tube model parameters, the molecular weight distribution of several samples has been determined. Concerning the transition to equilibrium, that is, entanglement recovery of the heterogeneous melt, this work examines the following two possibilities: (1) re-entanglement via ordinary reptation in dilated tubes and (2) re-entanglement by means of activated reptation. The former approach confines the chains into dilated tubes, that is, to tubes with a larger diameter than that at equilibrium, taking into account their partially entangled nature. Essentially, the model homogenizes φ_e, the initial (volume) fraction of entangled melt and permits molecular motions such as reptation in tubes that decrease in diameter with increasing time. This homogenization appears to work when φ_e is below a threshold value, which is about 0.4. For values larger than the threshold value, the proposed model performs poorly. Compared to the model prediction, the actual re-entanglement time is considerably longer, presumably because of the long time required for disentangled domains to maneuver themselves through the entangled fraction of the melt. In this regime, the activated reptation picture is more realistic. Further, the activated reptation picture appears to be applicable even below the threshold φ_e value, suggesting that re-entanglement occurs through activated reptation.

1. INTRODUCTION

The chain length or molecular weight (M_w) of a linear polymer chain has a drastic effect on its solution/melt dynamics as well as on the mechanical properties of fibers or tapes produced from such systems. To be more specific, for linear polyethylene (PE), mechanical properties such as tensile stress and modulus are known to increase with increasing molecular weight.[1−4] In this respect, molecular weights of the order of a million and above make PE chains available for demanding applications such as bulletproof vests.[5] Nevertheless, processability of the chains lessens with increasing M_w since the number of entanglements acting on a chain increases as well. Consequently, chain dynamics is slowed down with a subsequent increase of the viscosity.[6,7] Crystallization (solidification) from dilute solutions, that is, dissolution of the polymer chains in solvents in order to reduce the entanglement degree, provides a method to overcome this drawback.[8,9] However, this method is not environmentally friendly as it requires more than 90 wt % of solvent.

On the other hand, a unique method developed by Rastogi and co-workers allows the crystallization of ultra-high-molecular-weight PE (UHMW-PE) polymer chains from the melt.[10−14] Here, with the help of controlled synthesis at low temperatures, the crystallization rate is larger than the polymerization rate, facilitating chain growth in disentangled (semicrystalline) domains. It is reported that most of the entanglements present are formed during the early stages of polymerization (synthesis) before the nucleation for crystallization is reached.[4,10,15,16] As a result, a heterogeneous structure is obtained, often referred to as the disentangled nascent material, in which entanglements are mainly localized at the extremities of the crystalline domains.[4,10,15,16] Thus, upon heating, the regions close to crystals' extremities rapidly transform to entangled normal melt regions, whereas the remaining crystal cores stay disentangled, forming in this way a heterogeneous melt (nascent melt). (For a schematic representation of the nascent melt, see Figure 4.) This heterogeneous melt is in a nonequilibrium, metastable state as it comprises regions with different entanglement densities. With increasing time, it returns to an equilibrium (homogeneous) state where all regions are equally entangled, having the equilibrium entanglement molecular weight (M_e), typically found for non-UHMW-PE melts.

The aforementioned transition to equilibrium has been thoroughly investigated and confirmed by experimental means.[11−14] In more detail, the experiments reveal that the storage modulus of the heterogeneous melt increases with time until it reaches a value of approximately 2 MPa, after which a plateau zone is observed. This value corresponds to the entanglement plateau modulus of PE melts.[17,18] The increase

Received: June 4, 2019
Revised: October 28, 2019
Published: November 12, 2019

ACS Publications

Table 1. Polymerization Time and Temperature as Well as Ethylene Pressure for all Samples Considered in This Work, as Obtained from Refs[12−14]

samples	polymerization time (minutes)	polymerization temperature °C	ethyle pressure (bar)	cocatalysts
group A: A1, A2, A3, A4	2, 5, 10, 30	10	1.1	MAO
group B: B1, B2, B3	2, 10, 30	10	1.1	MAO + BHT
group C: C1, C2, C3, C4, C5	1, 2, 5, 10, 30	10	1.0	MAO
group D: D1, D2, D3, D4, D5	5, 15, 30, 60, 120	10	1.0	MAO

in G' is typically referred to as the modulus build-up. Moreover, linear rheology has been used to infer the molecular weight distribution (MWD) of those materials. More specific, small amplitude oscillatory shear (SAOS) measurements have been performed on the (initially) heterogeneous melt after its equilibration.[12−14] The obtained SAOS data were then fitted by a double reptation model, in particular the one of Mead,[19] inferring the MWD of the samples.[12−14] Nevertheless, parameterization consistency across the previous works was somewhat overlooked. It should be stressed that linear rheology is the only way to infer the MWD of extremely long chains since gel permeation chromatography (GPC) fails to give reliable results for molecular weights exceeding 2×10^6 g/mol because of the inhomogeneous dissolution of long chains in common GPC solvents.[20,21]

Despite the above-mentioned abundance of rheological observations on disentangled UHMW-PE, theoretical efforts on understanding the dynamics of such polymer systems, during and after the equilibration process, are sparse. Regarding equilibrated melts, Semenov and Rubinstein[22] proposed that above a critical molecular weight, excluded volume interactions dramatically slow down ordinary reptation, making it an activated process. According to the Semenov—Rubinstein (SR) theory, complete chain reorientation requires synergistic efforts of different chains.

Concerning nonequilibrated melts, the work of Vettorel and Kremer[23] studies the re-entanglement process by means of computer simulations (i.e., molecular dynamics). Here, the nascent melt is represented by an assembly of non-overlapping globules. The work reports that re-entanglement is independent of the position of the chain ends in the initial globular configuration. It also reports that the distribution of entanglements during the re-equilibration process is broad. Nevertheless, because of the immense computational time needed, the study actually focused on relatively short chains. In another work,[24] McLeish proposed an activated reptation process to describe the modulus build-up of a heterogeneous melt. According to McLeish, two opposing factors determine the re-entanglement time, namely, the free energy penalty associated with confinement of disentangled domains and the elastic (deformation) energy required to move the disentangled domains through the entangled ones.

This work contributes to the understanding of the UHMW chain dynamics in the following manner. As far as equilibrated melts are concerned, it compares the activated reptation theory of SR[22] and the typical reptation (tube) theory as implemented in refs.[25,26] Predictions of the SR theory (for the terminal relaxation time) strongly depend on the exact value that c takes (c is a model parameter of order unity). They can be similar to those of the ordinary theory or drastically different, depending on moderate changes in the value of c. Because of this ambiguity, this work adopts the usual tube model and shows that the experimental findings (SAOS measurements) can be described rather well by the usual tube model. Further, it determines the MWD of several samples using a single parameterization set for the model parameters. Most of the results do not differ significantly from those reported in earlier works.[12−14] It is to be noticed that this work does not claim that the tube model is superior to the SR model in describing the dynamics of UHMW chains.

With respect to nonequilibrated melts, the article examines whether the actual re-entanglement kinetics, as described by the (elastic) modulus build-up, can be reproduced by considering nonactivated reptation out of a dilated tube. In this molecular picture, entanglement recovery is viewed as the complementary process of chain reorientation. A scenario at which reptation occurs in a tube that decreases in diameter with increasing time is also examined. In either case, the proposed framework homogenizes the initial (volume) fraction of entangled melt (φ_e). Below a threshold value for φ_e, which is about 0.4, it provides a reasonable fit to modulus build-up observations. In contrast, it behaves poorly for the lowest molecular weights examined. For those molecular weights, φ_e is the highest, indicating that heterogeneity in the entanglement density must be definitely taken into account when φ_e is larger than 0.4. As it considers entanglement heterogeneity, the article also examines the ability of the activated reptation theory of McLeish[24] to quantitatively describe the experimental findings. It is shown that the theory can capture the actual measurements, provided that φ_e is assumed lower than the fraction suggested experimentally or the order 1 factors in the elastic and confinement free energies are considered different than unity.

2. MATERIALS AND METHODS

Four different groups of materials are considered in this work, hereafter, referred to as group A, B, C, and D. Groups A to D comprise four, three, five, and five samples, respectively. The synthesis and rheological characterization of all aforementioned samples have been reported previously. More specific, details about the materials of group A and group B can be found in ref 14. The synthesis and rheology of the samples of the two other groups (C and D) are reported in refs 13 and,[12] respectively. For each sample, Table 1 summarizes the most important information regarding material synthesis (i.e., polymerization time and temperature as well as ethylene pressure), as obtained from the corresponding references. In view of Table 1, it is worth noting that the use of the term “group” might be misleading as all materials are of the same kind, i.e. linear polyethylene chains. In fact, since conditions other than the polymerization time are the same for groups A, C, and D, one would expect polymerizations of the same time to produce identical results with respect to MWD and φ_e. In practice, the results are similar but not the same, presumably due to the statistical character of the polymerization reaction.

Concerning the rheological characterization, as detailed in refs,[12−14] it has been carried out in the linear flow regime, that is, at a strain that lies well in the linear regime. All build up measurements refer to a temperature of 160 °C and to an angular frequency of 10 rad/s, which, in most cases, lie within the entanglement plateau zone. The latter has been probed by means of SAOS, with measurements being performed after reaching the

Table 2. M_w and PDI as Obtained by Fitting SAOS Data with the Tube Model[a]

samples	polymerization time (minutes)	M_w kg/mol	PDI index
group A: A1, A2, A3, A4	2, 5, 10, 30	500, 1200, 2350, 6100 (700, 1200, 2300, 5600)	1.2, 1.5, 1.7, 2.5 (1.3, 2, 1.9, 3.2)
group B: B1, B2, B3	2, 10, 30	390, 1900, 5000 (600, 1800, 4200	1.2, 1.8, 2.75 (1.2, 1.8, 2.4)
group C: C1, C2, C3, C4, C5	1, 2, 5, 10, 30	-, -, 1350, -, - (300, 600, 1400, 2500, 5100)	-, -, 2.2, -, - (1.4, 1.7, 2.5, 2.4, 2.5)
group D: D1, D2, D3, D4, D5	5, 15, 30, 60, 120	780, 2300, 4400, 8500, 12 000 (970, 2370, 4190, 5630, 7110)	1.5, 2, 2.5, 3.5, 3.5 (1.8, 2.4, 2.5, 3.2, 3.0)

[a] Values in parenthesis correspond to the values reported in previous works.

equilibrium state of the polymer melt. Note that this is not the case for samples D4 and D5 for which equilibration was not achieved within the experimental time window. Therefore, SAOS data for these two samples correspond to a metastable state.

Concerns related to the reliability of the modulus build-up data are discussed in Section S1 extensively. The information provided in Section S1 of the Supporting Information strengthens the notion of re-equilibration reflecting chain re-entanglement rather than being an artefact such as melt homogenization due to bubble dissolution.[27] Air inclusion can occur when sintering[28] UHMW-PE powder to disks for rheology measurements. In summary, the build-up data reported in refs[12−14] is unlikely to be attributed to melt homogenization for the following reasons: (1) The surface morphology of disentangled UHMW-PE (Dis-PE) is not reminiscent of a foam, as revealed by optical micrographs before and after rheology (Figures S1, S2, S4, and S5). (2) Dis-PE powder has higher porosity[1] than E-PE powder (commercially entangled UHMW-PE) leading to better densification (Figures S6 and S7). (3) The superior densification of Dis-PE compared to E-PE powder as well as the enhanced chain mobility upon melting lead to better fusion of the Dis-PE powder, when sintering occurs in the melt. This is confirmed by the absence of grain boundaries in Dis-PE sintered in the melt[20,29] (Figure S8). (4) Even when sintered below the melt, Dis-PE contains limited amount of grain boundaries[20] (Figure S9). (5) The modulus build-up is suppressed in protonated-deuterated Dis-PE block copolymers[30] because of the tendency of protonated and hydrogenated species to phase separate[31,32] (Figure S10a). It is also suppressed in composites of reduced graphene oxide nanosheets (rGON) with Dis-PE[33] (Figure S10b). This suppression is attributed to the strong interaction of the PE chains with the rGON filler. (6) SAXS studies on Dis-PEs reveal that during equilibration, structural changes on the 60 nm length scale ($\sim R_g$ of the chains) occur (Figure S12). Such changes do not occur at equilibrated samples (Figure S13). (7) Finally, the molecular origin of re-entanglement is further strengthened by DSC studies on Dis-PE samples.[10,16,34,35] Such studies demonstrate remarkably good correlation between "DSC build-up" and rheology build-up curves for Dis-PE samples[16] (Figure S14).

3. LINEAR RHEOLOGY OF EQUILIBRATED UHMW MELTS: MWD DETERMINATION USING ORDINARY REPTATION THEORY

Before investigating the nonequilibrated melts, the focus will be on the equilibrated ones, perceived after leaving the nonequilibrated melts at 160 °C for a sufficiently long time (typically more than 10 h[12−14]). As aforementioned, Semenov and Rubinstein proposed that reptation becomes an activated process when the chains have ultrahigh molecular weight.[22] In this respect, the SAOS data of the samples of Table 1 provide a good opportunity to examine the performance of the SR model. However, as detailed in Section S2, it is impossible to judge the performance of the model. This is because the SR model is based on scaling arguments meaning that its predictions for the terminal reorientation time are very sensitive to the values that a model parameter takes; depending on the exact value, predictions can be similar or totally different than the predictions of the tube model, which assumes nonactivated reptation (among other reorientation mechanisms). We stress that the possibility that the SR model describes the SAOS observations cannot be excluded. Because of the aforementioned uncertainty, however, it was decided to focus on the tube model only. In conclusion, the naive analysis presented in Section S2 by no means excludes the possibility of the SR model having superior performance over the tube model in describing the dynamics of UHMW chains. In other words, the possibility that excluded volume interactions influence the dynamics of UHMW chains is not rejected. It is not the purpose of this work to perform a detailed comparison between the SR model and the tube model. In this respect, the use of the tube model in the remaining part of the manuscript does not justify the applicability of the model for UHMW chains. The tube model together with SAOS data of equilibrated samples serve as a tool to provide a good estimation of the molecular weight and polydispersity (PDI) of the samples. Thus, the values reported in Table 2 below should be treated with caution. Considering that the applicability of the tube model is not justified and that the MWDs cannot be experimentally determined with high accuracy for molecular weights in the order of 2000 kg/mol and above, the M_w and PDI values of Table 2 should be treated as approximate rather than absolute values. As shown in Section 5 as well as in Sections S5 and S6, variations from the values reported in Table 2 are possible. Nevertheless, such variations will not influence, on a qualitative level, the analysis and theoretical results related to the modulus build-up (Section 4). Since the main purpose of this work is to gain a first understanding of the molecular mechanism of re-entanglement, detailed considerations such as the precise MWD or the potential effect of excluded volume interaction are disregarded. The influence of such details will of course be crucial for a complete quantitative description of both the equilibrium and nonequilibrium rheological response of UHMW-PE chains.

Figures 1 and 2 present the general features of the tube model, for UHMW-PE chains, as obtained from the so-called BOB (branch on branch) software.[26] More specific, Figure 1 presents the dynamic moduli, and Figure 2 shows the corresponding slopes of the viscous (loss) moduli. Figure 1 also includes the experimental data of all samples of group A. Concerning Figure 2, it includes the slopes of the experimental G'' data presented in Figure 1. Note that all predictions in Figures 1 and 2 have been obtained using $M_{e,eq} = 1250$ g/mol, $G_N^0 = 2.2$ MPa, and $\tau_{e,eq} = 5 \times 10^{-8}$ s because these values better fit the experimental data as will be shown below. Model predictions refer to average molecular weights of 500, 1000, 2000, and 4000 kg/mol. Regarding the model outcomes for polydisperse chains, they have been obtained using log-normal distributions. Such distribution functions are typically used to capture the actual MWD of PE and isotactic polypropylene (iPP) polymer melts.[36−39]

DOI: 10.1021/acs.macromol.9b01152
Macromolecules 2019, 52, 8849−8866

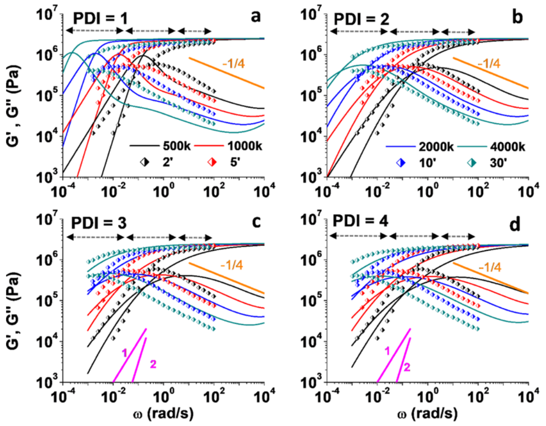

Figure 1. Tube model predictions for various molecular weights and PDIs. The anticipated power law behavior of G'' in the CLF regime is shown as a line with a slope of −1/4. The expected power laws for G' and G'', indicative of ordinary diffusion in the terminal regime, are also shown. The data for samples A1 to A4 are also included for comparison. Temperature is 160 °C. $M_{\mathrm{e,eq}} = 1250$ g/mol, $G_{\mathrm{N}}^{0} = 2.2$ MPa, and $\tau_{\mathrm{e,eq}} = 5 \times 10^{-8}$ s.

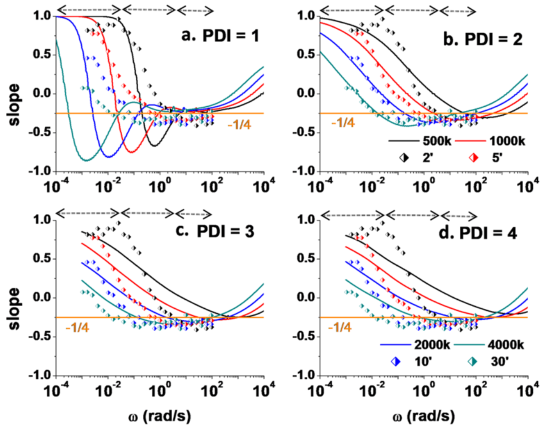

Figure 2. Corresponding slopes of all G'' predictions and data presented in Figure 1. Here, the CLF regime appears as a horizontal line. Temperature is 160 °C.

Focusing first on the tube model predictions for monodisperse melts, three distinct regimes are readily identified in Figures 1a and 2a. Here, the dashed arrows are meant as an eye guide for the reader and indicate the three regimes for the line referring to 500 kg/mol. At intermediate frequencies, where G' exhibits a plateaulike behavior, G'' manifests power law behavior with the slope of the curves being −1/4 in a log−log representation. For well-entangled chains, this slope is anticipated, and it is the signature of contour length fluctuations (CLFs).[6,26,40] (Nevertheless, these fluctuations do not affect the terminal relaxation significantly since the chains are extremely long.[6]) Moving to lower frequencies, G' begins to drop, indicating that some chain sections have escaped their initial confinement. The power law behavior of G'' changes from $G''(\omega) \approx \omega^{-1/4}$ to $G''(\omega) \approx \omega^{-1/2}$. Eventually G' and G'' cross over, marking the end of the second regime. The cross-over frequency corresponds to the inverse of the reptation time of the monodisperse chains. At even lower frequencies, a third regime appears. Here, ordinary diffusion takes place, with G' and G'' following power law behavior (slopes of 2 and 1, respectively, in a log−log representation).

Figures 1b−d and 2b−d examine how the tube model predictions, in the aforementioned three regimes, change with increasing PDI. Dashed arrows indicate the same regimes as in Figures 1a and 2a for the curve referring to 500 kg/mol. Focusing on the theoretical predictions, Figures 1b−d and 2b−d demonstrate that, with increasing PDI, the regime over which CLF dominates the G'' response narrows. This is because the terminal relaxation of low M_{w} chains overlaps with the CLF relaxation of chains of higher M_{w}. Moreover, the second regime where data for monodisperse systems exhibit a slope of −1/2 disappears. Subsequently, the cross-over of G' and G'' appears more like a zone region rather than a distinct point (frequency).

Shifting attention to the comparison between data and model predictions, it is obvious from Figures 1a and 2a that the samples are not monodisperse. It also becomes clear that samples A1−A4 are not highly polydisperse. This is because in Figures 1 and 2, the SAOS measurements are better described by the model outcomes for a PDI index of 2. The only obvious exception is sample A1, which appears to have a PDI between 1 and 2. Expectably, increasing polymerization time translates to chains of higher molecular weight. Therefore, one would anticipate the molecular weights of samples A1 to A4 to obey the following order: A4 > A3 > A2 > A1. This is also supported by the SAOS data, that is, samples obtained using longer polymerization times manifest a lower cross-over frequency. According to the tube model predictions shown in Figure 2, the M_{w} of samples A1 to A4 should be in the order of 500, 1000, 2000, and 4000 kg/mol, respectively. The exact M_{w} and PDI values will be determined below. In conclusion, Figures 1 and 2 show that it is possible to describe the experimental data using ordinary tube theory.

Because of ease of computational implementation, rather than BOB,[26] another popular implementation of the tube model was chosen for the MWD determination. More specific, the time marching algorithm (TMA) of van Ruymbeke et al.[25] was selected. Both models are based on similar physics and give similar results (see Section S3). The adopted procedure for the MWD determination is as follows. SAOS data of three grades were considered in order to determine the model parameters M_{e}, G_{N}^{0}, and τ_{e}. More specific, the data corresponding to samples A1, C3, and D1 were selected. A1 and D1 were chosen because they have the shortest polymerization time among the other samples of the same group, meaning that the lowest molecular weight is anticipated for them. The reasoning for choosing the SAOS data of the shortest chains is that the original tube model (nonactivated reptation) would still hold for those molecular weights, even if it would fail for larger molecular weights. Sample C3 was chosen because it is the only sample from group C for which SAOS data were available.[13]

Model predictions for numerous combinations of $M_{\mathrm{e,eq}}$, G_{N}^{0}, and $\tau_{\mathrm{e,eq}}$ as well as M_{w} and PDI were obtained (see Figure S17 of Section S4). For each combination, errors for the loss modulus and the storage modulus as well as for the complex viscosity were calculated separately. The minimum of those three errors was considered as the total error between theoretical outcomes and measured values. Combinations producing a large total error were excluded from further minimization, at which the allowed combinations of molecular parameters, M_{w} and PDI, were narrowed down further (see

Figure S18 of Supporting Information). As detailed in Section S4 of the Supporting Information, the combination of tube model parameters that gave the least error was $M_{e,eq}$ = 1250 g/mol, G_N^0 = 2.2 MPa, and $\tau_{e,eq} = 5 \times 10^{-8}$ s. The applicability of this parameterization for non-UHMW-PE melts[17,18,36,41,42] is examined in Section S5.

Having obtained the values of $M_{e,eq}$, G_N^0, and $\tau_{e,eq}$, MWD determination for the other samples was carried out by varying the M_w and PDI values only. Figure 3A–D present the best fit for the samples of groups A to D, respectively. Symbols refer to measurements while lines refer to model predictions. Table 2 summarizes the obtained M_w and PDI values for all samples of groups A to D. These values have been used in Section 4 below, where theoretical predictions for the modulus build-up are compared against experimental findings. Note that Table 2 includes M_w and PDI values obtained from previous characterization using the Mead model.[19] These results are reported in parenthesis. It is to be noticed that the M_w and PDI values of Table 2 should be treated with some caution since the applicability of the tube model as well as its parameterization cannot be fully justified (see Section 5 below as well as Sections S5 and S6 of the Supporting Information).

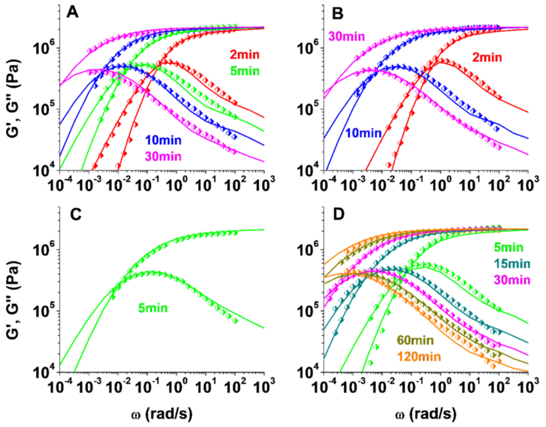

Figure 3. MWD determination for all samples of groups A–D, for which SAOS data were available, using the tube model. Symbols refer to SAOS data while lines refer to theoretical predictions. Temperature is 160 °C. The values of the molecular parameters are $M_{e,eq}$ = 1250 g/mol, G_N^0 = 2.2 MPa, and $\tau_{e,eq} = 5 \times 10^{-8}$ s. For M_w and PDI values, see Table 2.

Two more points should be made clear here. First, SAOS data for samples C1, C2, C4, and C5 are not available in ref 13; on the basis of the good agreement with the previously reported values for sample C3 (see Table 2), the values reported in ref 13 will be used hereafter for samples C1, C2, C4, and C5. Second, the SAOS data of samples D4 and D5 have been shifted vertically as to match the plateau values of samples D1–D3. The vertical shift factors applied were 1.2 and 1.5, respectively. As mentioned in Section 2, equilibration of samples D4 and D5 was not achieved within the build-up measurement meaning that the samples contain chains or chain portions that are not fully entangled. Thus, the obtained M_w and PDI values listed in Table 2 are approximate. Within the experimentally accessible frequencies ($2 \times 10^{-4} < \omega < 10^2$), the shape of the SAOS data of the nonequilibrated samples is not expected to differ significantly from the shape that would have been obtained if samples were equilibrated. Nevertheless, diffusion at frequencies below the cross-over most likely will be interrupted by the equilibration of the partially entangled chains/chain sections. The appearance of a shoulder would be expected if measurements could be carried out at very low frequencies. Thus, the actual M_w and PDI could be larger than those obtained from Figure 3D.

4. LINEAR RHEOLOGY OF UHMW CHAINS IN NONEQUILIBRIUM MELT STATE: MODELLING THE ELASTIC MODULUS BUILD-UP

4.1. Simple Expression for the Elastic Modulus Build-Up. It is generally accepted that fast flows can produce disentanglement, which is followed by re-entanglement when the flow is ceased.[43−45] To describe the re-entanglement process, research works on this topic make use of an equation of the form[43−45]

$$\frac{d\Psi}{dt} = -\frac{1}{\tau_b(t)}(\Psi - 1) \tag{1}$$

where $\Psi(t)$ (=$Z(t)/Z_{eq}$) denotes the fraction of entanglements acting on the chains at time t, with $Z(t)$ being the actual number of active entanglement at time t and Z_{eq} being the number of entanglements at equilibrium (a time independent quantity). Thus, $\Psi(t)$ can be re-expressed in terms of the entanglement molecular weight as $\Psi(t) = M_{e,eq}/M_e(t)$, with $M_{e,eq}$ and $M_e(t)$ denoting the entanglement molecular weight at equilibrium and at time t, respectively. The form of eq 1 is general; the re-equilibration time, τ_b, varies depending on the particular implementation and/or polymer topology.[43−45] It can be constant or time dependent. In this work, eq 1 is adopted, and the re-entanglement time is modified as to reflect the equilibration process of the heterogeneous UHMW-PE melts.

In view of the fact that model predictions are eventually compared against G' build-up measurements, it is convenient to rewrite eq 1 as

$$\frac{dG'(t)}{dt} = -\frac{1}{\tau_b(t)}(G'(t) - G_N^0) \tag{2}$$

where G_N^0 is the (equilibrium) entanglement plateau modulus. In arriving to eq 2, the expression $M_{e,eq}/M_e(t) = G'(t)/G_N^0$ has been used, assuming that the inversely proportional relation between the entanglement molecular weight and elastic modulus holds even out of equilibrium. If the re-equilibration time is assumed constant, eq 2 has the analytical solution

$$G'(t) = G_N^0 + (G_0 - G_N^0)e^{-t/\tau_b} \tag{3}$$

where $G_0 = G'$ $(t = 0)$ corresponds to the value of the storage modulus at the beginning of the build-up measurement. Note that eq 3 can provide a good match to the build-up data of all samples if τ_b is treated as an arbitrary fitting parameter. As can be seen in Figure S24 of Section S7, the fit can be further improved if PDI is indirectly taken into account by modifying the exponential term of eq 3 so that $G'(t)$ becomes

$$G'(t) = G_N^0 + (G_0 - G_N^0)e^{-\left(\frac{t}{\tau_b}\right)^{\beta}} \tag{4}$$

where both τ_b and β act as fitting parameters. Having obtained these values, the average re-entanglement time can be defined through the expression

$$\overline{\tau_{re}} = \tau_b\Gamma(1/\beta)/\beta \tag{5}$$

DOI: 10.1021/acs.macromol.9b01152
Macromolecules 2019, 52, 8849−8866

where $\Gamma(x)$ is the gamma function. Equation 5 can be used for the estimation of the re-entanglement times (see Section S7). As the objective of this work is to gain molecular insight about the re-entanglement process, rather than provide a successful fit to the data only, Section 4.2 below examines whether the re-entanglement process can be viewed as the complementary process of chain reorientation. More specific, it investigates if the observed re-entanglement kinetics can be described by means of tube escape from dilated tubes.

4.2. Re-entanglement via Means of Tube Escape from Dilated Tubes.

The most plausible molecular picture for the structure of the nascent material upon melting is illustrated schematically in Figure 4 (right top). The structure is heterogeneous, comprising regions rich in disentangled chain sections and domains rich in entangled chain sections, with the entanglement density of those regions being the equilibrium one.[10,16,24] In this respect, a given polymer chain of the heterogeneous melt can be thought of as being confined at its two extremities only (Figure 4, bottom right). At those entangled sections, the molecular weight between entanglements corresponds to that at equilibrium. In contrast, inner sections of the chain consist of disentangled domains.

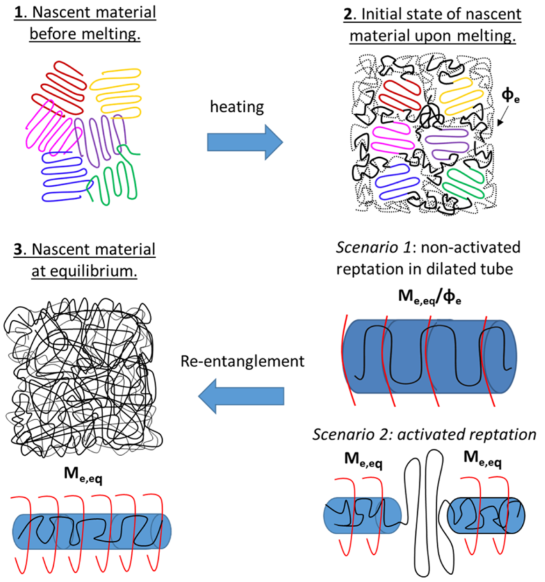

Figure 4. (Top) Schematic representation of the nascent material prior to entanglement recovery, below and above the melt temperature. The structure is heterogeneous, meaning that there are domains with high and low entanglement density. (Bottom) Molecular scenarios of entanglement recovery (right). Scenario 1: the initial entangled fraction, φ_e, is evenly distributed along the chain contour, creating confinement in a dilated tube. Re-entanglement occurs as chains reptate out of dilated tubes. Scenario 2: the initial entangled fraction remains heterogeneous. Re-entanglement occurs by means of activated reptation. Eventually, all chain sections experience the same (equilibrium) confinement (left).

Although the actual structure of the melt is heterogeneous, here, a molecular scenario that homogenizes φ_e, the initial fraction of entangled melt, is examined. As shown in Section S10, there are no fully disentangled chains after this homogenization. All assumptions of the proposed approach are the following:

1. Consider a given chain of the nascent melt. φ_e is evenly distributed along the chain (see Figure 4—Scenario 1) This oversimplified view overlooks the heterogeneous nature of the melt. On the other hand, it takes into account the disentangled (partially entangled) nature of the chains. φ_e is determined from the build-up data, that is, $\varphi_e = G_0/G_N^0$.
2. Re-entanglement is viewed as the complementary process of chain reorientation. The latter is assumed to be driven by the chain ends. Thus, as the chains move out of the dilated tubes via reptation, they reform entanglements with other matrix chains.
3. The inversely proportional relation between the entanglement molecular weight and the elastic modulus holds during entanglement recovery. At equilibrium, $G' \approx G_N^0 \approx 1/M_{e,eq}$.

In view of assumptions 1 and 2 above, τ_{re}, the re-entanglement time is expressed as

$$\tau_{re} = \begin{cases} \tau_b(t) = 3\tau_0\left(\dfrac{N_{e,eq}}{\mathbf{\Psi}(t)}\right)^2\left(\mathbf{\Psi}(t)\dfrac{M_w}{M_{e,eq}}\right)^3 = 3\tau_{e,0}Z_{eq}{}^3\mathbf{\Psi}(t) & \text{(6a)} \\ \quad = \tau_{b,0}\dfrac{G'(t)}{G_N^0} & \\ \tau_b = 3\tau_0\left(\dfrac{N_{e,eq}}{\mathbf{\Psi}(0)}\right)^2\left(\mathbf{\Psi}(0)\dfrac{M_w}{M_{e,eq}}\right)^3 = 3\tau_{e,0}Z_{eq}{}^3\mathbf{\Psi}(0) = \tau_{b,0}\varphi_e & \text{(6b)} \end{cases}$$

where $\tau_{b,0}$ $(=3\tau_{e,0}Z_{eq}{}^3)$ is the unperturbed reptation time and $\Psi(t)$ is the current fraction of active entanglements. Equations 6 a and 6b refer to a time dependent and a constant reptation time, respectively. Note that in the former scenario, the newly created tube segments are assumed to contribute to subsequent relaxation of the chains. On the other hand, in the latter scenario, newly created tube segments do not contribute to further chain reorientation; here, entanglement reformation is essentially the complementary process of chain reorientation. This scenario is consistent with ref 46 and the conventional picture of orientation relaxation in tube theory.[6,7,25,26]

Equations 6a and 6b are incorporated in the tube model framework of the TMA.[25,47,48] According to this framework, the dynamics of the tube escape mechanisms of reptation and CLF are, respectively, governed by the following probabilities

$$p_{rep}(x_i, t) = \sum_{p\ \mathrm{odd}} \frac{4}{p\pi}\sin\left(\frac{p\pi x_i}{2}\right)\mathrm{e}^{-p^2 t/\tau_{b(t)}} \tag{7a}$$

$$p_{fluc}(x_i, t) = -\frac{t}{\tau_{fluc}(x_i, t)} \tag{7b}$$

where x_i is a normalized curvilinear variable that represents the primitive path segments. Further, $\tau_{fluc}(x_i,t)$ is the CLF relaxation time of segment x_i at time t. The explicit formula for $\tau_{fluc}(x_i,t)$ can be found in refs.[47,48] From eq 7a, the tube survival probability, $\Psi^{TUBE}(t)$, can be calculated as follows

$$\mathbf{\Psi}^{TUBE}(t) = \sum_i w_i \int_0^1 p_{rep}(x_i, t)p_{fluc}(x_i, t)\mathrm{d}x_i \tag{8}$$

where w_i is the volume fraction of component (molecular weight) i. Constraint release (CR) effects on chain relaxation (reorientation) are treated in the usual manner,[25,47,48] that is, $\Phi(t)$, the CR contribution to chain reorientation is estimated using the expression

$$\Phi(t) = \max[\mathbf{\Psi}^{\mathrm{TUBE}}(t), \Phi(t - \Delta t)(t - \Delta t/t)^{1/2}] \tag{9}$$

where Δt is the time step in the algorithm. At $t = 0$, $\Phi(0) = 1$.

According to assumption 2 above, tube escape translates to entanglement recovery. In this respect, $\mathbf{\Psi}^{\mathrm{TUBE}}(t)$ should be related to $\Psi(t)$, the fraction of active entanglements. CR does not directly contribute to tube escape. However, it indirectly accelerates the reptation of a test chain since the tube it was initially confined within widens with increasing time, reflecting the relaxation of the surrounding chains. In this respect, $\Phi(t)$ should also be related to $\Psi(t)$. Equation 10 below provides this interrelation

$$\mathbf{\Psi}(t) = \varphi_{\mathrm{e}}\mathbf{\Psi}^{\mathrm{TUBE}}(t)\Phi(t) + (1 - \mathbf{\Psi}^{\mathrm{TUBE}}(t)\Phi(t)) \tag{10}$$

Equation 10 has the correct asymptotic behavior, that is, at $t = 0$, the tube survival probability and the CR function are unity, thus $\Psi(t) = \varphi_{\mathrm{e}}$. At $t \to \infty$, the tube survival probability vanishes, meaning that $\mathbf{\Psi}^{\mathrm{TUBE}}(t \to \infty) = 0$, therefore the fraction of active entanglements is unity. If CR is overlooked, eq 10 reduces to

$$\mathbf{\Psi}(t) = \varphi_{\mathrm{e}}\mathbf{\Psi}^{\mathrm{TUBE}}(t) + (1 - \mathbf{\Psi}^{\mathrm{TUBE}}(t)) \tag{11}$$

that exhibits the correct asymptotic behavior too. Finally, using the definitions $\Psi(t) = G'(t)/G_{\mathrm{N}}^{0}$ and $\varphi_{\mathrm{e}} = G_0/G_{\mathrm{N}}^{0}$, the expression for the modulus build-up in this second approach reads

$$G'(t) = G_0\mathbf{\Psi}^{\mathrm{TUBE}}(t)\Phi(t) + G_{\mathrm{N}}^{0}(1 - \mathbf{\Psi}^{\mathrm{TUBE}}(t)\Phi(t)) \tag{12}$$

In the absence of second-order effects such as CR, there should be consistency between the two approaches. In other words, eqs 2 and 12 should give the same results when the reptation time is given by either eq 6a or eq 6b. Figure 5 compares the two methods for three different molecular weights. Predictions of the second approach (eq 12 with $\Phi(t) = 1$) are presented by lines, and predictions of the first method (eq 2) are shown by symbols (circles and crosses for $\tau_{\mathrm{b}}(t)$ and τ_{b}, respectively). In obtaining the predictions of the second method, fast reptative (subreptative) modes have been neglected, that is, $p = 1$ in eq 7a, since the first method omits such a second-order effect. According to Figure 5, the two approaches give identical results for a constant reptation time. Concerning the time-dependent reptation case, discrepancies between the two methods can be seen. Nevertheless, these discrepancies are not large enough to render the two methods inconsistent. For this reason and since it provides a framework to which secondary effects can be accommodated, the TMA-based approach is considered in the remainder of this section.

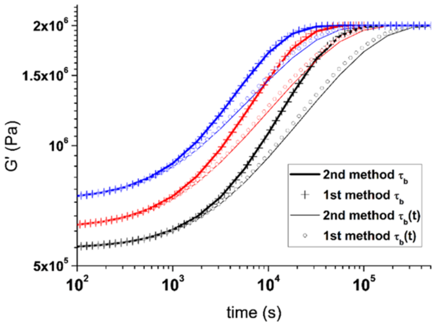

Figure 5. Comparison of the outcomes of eqs 2 and 12 [with $\Phi(t) = 1$] in the absence of second-order effects such as PDI, subreptative modes, CLF, and CR. Symbols refer to eq 2 while lines refer to eq 12. Predictions are shown for both constant and time-dependent reptation scenarios. Here, $M_{\mathrm{e,eq}} = 1200$ g/mol, $G_{\mathrm{N}}^{0} = 2.2$ MPa, and $\tau_{\mathrm{e,eq}} = 1.2 \times 10^{-8}$ s.

Figures 6−9 compare the predictions of eq 12 against experimental findings for all samples of Table 1. They have been obtained using $M_{\mathrm{e,eq}} = 1250$ g/mol, $G_{\mathrm{N}}^{0} = 2.2$ MPa, and $\tau_{\mathrm{e,eq}} = 5 \times 10^{-8}$ s, that is, the parameterization obtained in Section 3. In Figures 6−9, experimental data are shown as symbols. They have been reproduced from refs.[12−14] Note that for samples C1, C2, C4, and C5 the average molecular weight and PDI values correspond to the ones reported in ref 13 since SAOS data were not available for those samples. The exact values can be found in Table 2 (in parenthesis). As mentioned in Section 3, for sample C3, for which data were available, the difference between the M_{w} and PDI values determined in this work and those reported in ref 13 are small. Finally, note that

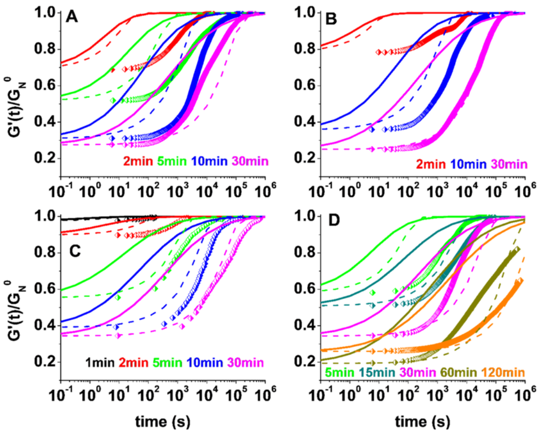

Figure 6. Comparison of model outcomes (eq 12—lines) and build-up measurements (symbols) for the samples of groups A to D. Subreptative modes and PDI are included. CLF and CR are ignored. Dashed and solid lines refer to indirect and direct PDI treatments. The reptation time is assumed constant.

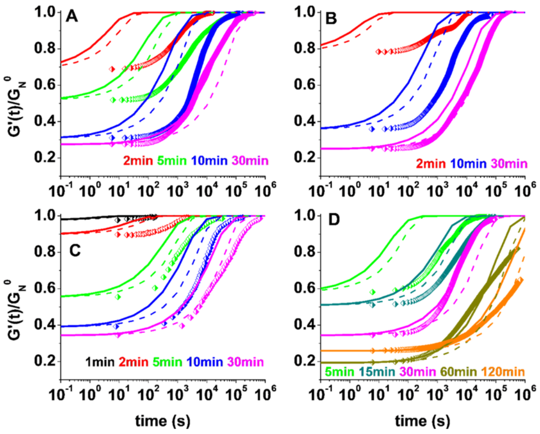

Figure 7. Comparison of model outcomes (lines) and build-up measurements (symbols) for the samples of groups A to D. Subreptative modes are included. PDI is treated using the indirect approach. The reptation time is assumed constant. Dashed and solid lines are obtained in the absence and presence of CR, respectively.

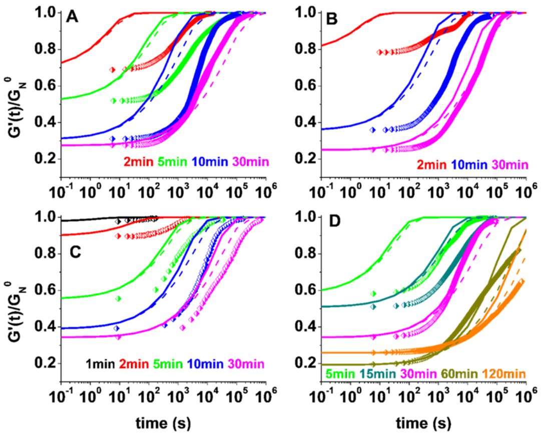

Figure 8. Comparison of model outcomes (eq 12—lines) and build-up measurements (symbols) for the samples of groups A to D. Subreptative modes are included as well as CR. PDI is treated using the indirect approach. Dashed and solid lines correspond to the time-dependent and "constant" reptation times, respectively. $M_{e,eq}$ = 1250 g/mol and $\tau_{e,eq} = 5 \times 10^{-8}$ s.

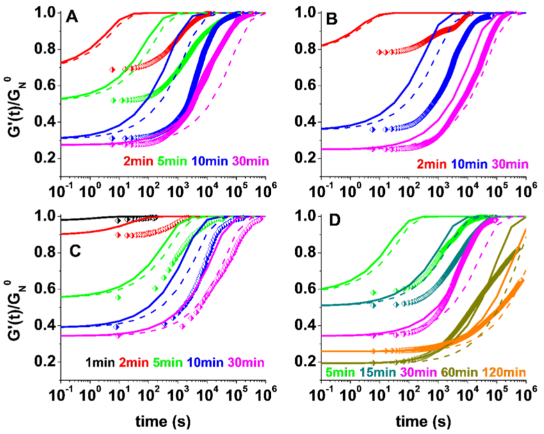

Figure 9. Comparison of model outcomes (eq 12—lines) and build-up measurements (symbols) for the samples of groups A to D. Subreptative modes are included as well as CR. PDI is treated using the indirect approach. Solid lines are the same as in Figures 7 and 8. Dashed lines refer to equilibrium melt dynamics. $M_{e,eq}$ = 1250 g/mol and $\tau_{e,eq} = 5 \times 10^{-8}$ s.

in obtaining the theoretical results of Figures 6–9, CLFs have been neglected. This is because they do not affect the predictions significantly; as readily seen in Figure S26 of Section S8, CLF influences the onset of the build-up curves, producing a moderate speed up of the re-equilibration process at those early stages only.

Figure 6 focuses on PDI treatment. In this figure, theoretical predictions appear as lines and have been obtained assuming a time-independent reptation time. Notice that CLF is disregarded. The same applies for CR, that is, $\Phi(t) = 1$ in eq 12. Solid lines refer to a scenario at which PDI effects are accounted for directly. This means that the samples are represented by log-normal distributions having the average M_w and PDI reported in Table 2; the contribution of each component (M_{wi}) to the overall tube survival probability is calculated explicitly in accordance to eq 8. The equilibrium reptation time $3\tau_{e,0}Z_{eq,i}^{3}$ of every component has been accelerated by φ_e. On the other hand, dashed lines have been obtained accounting for PDI indirectly. Here, the melt is essentially represented by one effective mode (molecular weight). The equilibrium reptation time of this mode is assumed to be the average reptation time of the distribution; that is, $\overline{\tau_{b,0}} = \sum w_i 3\tau_{e,0}Z_{eq,i}^{3}$. As in the direct approach, this average reptation time has been multiplied by φ_e.

Figure 6 reveals that the indirect approach compares better with the experimental results. It also reveals that, in either approach, the model performs better with increasing (decreasing) polymerization time/molecular weight (φ_e). For example, the dashed lines for samples B3 and C5, referring to polymerization time of 30 min, compare very well with the corresponding data. In contrast, all dashed lines that refer to polymerization times of one and 2 min exhibit the largest discrepancy. These two findings suggest that the shorter the chain, the most unrealistic the entanglement homogenization assumption is. This homogenization seems to underestimate the reptation time of those chains; compared to model predictions, in reality, the chains need much longer times to fully reorient. Presumably, movement of the disentangled chain sections is prohibited (delayed) by the surrounding entangled matrix as proposed by the theory of McLeish.[24] In other words, it appears that re-entanglement occurs through activated reptation.

Coming back to the two approaches for PDI, the reason the direct approach fails becomes now apparent. The reptation time of the short chains of the distribution is severely underestimated. Hence, these chains contribute to entanglement recovery much faster than they do in reality. Another reason behind the poor performance of the direct method could be the assumption of uniform dilation for all molecular weights. Overall, the proposed model performs reasonably well for polymerization times of 15, 30, 60, and 120 min, when PDI is treated in an indirect manner. In some occasions, the model also performs quite well for polymerization times of 5 and 10 min (samples C3 and C4). Nevertheless, for all groups, the model underperforms severely at the short and intermediate polymerization times (high φ_e values). In other words, it seems that there is a critical value for φ_e, above which the heterogeneity of the sample dramatically suppresses ordinary reptation of the chains. The determination of this critical value will be discussed in Figure 10 below.

Figure 7 focuses on the effect of CR. Predictions in the absence of CR are presented as dashed lines, whereas predictions in the presence of CR are shown by solid lines. In either case, PDI is accounted for by the indirect approach for the reasons explained above. The reptation time is considered constant; that is, it is given by $\overline{\tau_{b,0}} = \sum (w_i 3\tau_{e,0}Z_{eq,i}^{3})\varphi_e$. Nevertheless, in the presence of CR, this reptation time speeds up indirectly as the initial confinement lessens with increasing time. Further, CLFs are neglected. Hence, the dashed lines in Figure 7 are the same as the dashed lines in Figure 6. From Figure 7, it becomes apparent that CR accelerates the re-entanglement time moderately as it accelerates the overall chain reorientation. Nevertheless, from a qualitative standpoint, the performance of the model is independent of the inclusion or exclusion of CR. The model behaves reasonably well for long polymerization times but fails for intermediate and fast polymerization times. From a quantitative standpoint, inclusion of CR worsens the model performance for intermediate and fast polymerization times since CR speeds up re-entanglement.

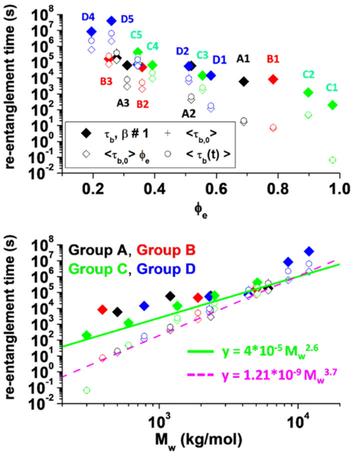

Figure 10. Re-entanglement times as a function of φ_e (top) as well as a function of weight-average molecular weight (bottom). Filled diamonds correspond to the experimental build-up timescales. Crosses correspond to the average reptation time at equilibrium. Unfilled diamonds and circles indicate re-equilibration by means of reptation in dilated tubes under the assumption of constant and time-dependent reptation times, respectively (see 6a).

Figure 8 compares the model predictions in the presence of CR, using "constant" and time-dependent reptation times in accordance with eqs 6a and 6b, respectively. Solid lines refer to the former scenario and are the same as the ones in Figure 7. Dashed lines refer to the latter scenario. Since CR is active, the "constant" reptation time is not truly constant during the computations but speeds up moderately with increasing time. Thus, in this case, the term "constant" is used to emphasize the independence of the reptation time on $\Psi(t)$, the current fraction of active entanglements. From Figure 8, it is obvious that entanglement recovery occurs faster when the reptation time is considered "constant." Here, τ_b is determined according to eq 6a, accounting for PDI indirectly. In other words, the reptation time is given by $\overline{\tau_{b,0}} = \sum (w_i 3\tau_{e,0} Z_{eq,i}{}^3)\varphi_e$, that is, the (equilibrium) average reptation time is speeded up by a factor of φ_e, reflecting the confinement in dilated tubes. As aforementioned, $\overline{\tau_{b,0}}$ decreases moderately with increasing time because of CR.

Continuing the discussion of Figure 8, in the time-dependent scenario, the reptation time is calculated in accordance with eq 6b. Therefore, it depends on $\Psi(t)$, a quantity that increases as time goes on. Here, chain relaxation (reorientation) takes place in a tube that decreases in diameter with increasing time. Thus, reptation slows down with increasing time, leading to moderately larger re-entanglement times. Nevertheless, the difference between the two approaches becomes less important with decreasing polymerization time as the initial fraction of entangled melt is closer to the equilibrium value ($\varphi_e = 1$). Focusing on polymerization times longer than 15 min, for which the model performs better, the time-dependent approach, overall, compares better with the experimental data. The only exceptions are the samples A4 and D3 for which the comparison worsens. Obviously, the time-dependent scenario performs better at the intermediate polymerization times of 5, 10, and 15 min since the actual reptation time of the chains is less severely underestimated.

Figure 9 reproduces the solid lines of Figure 8, that is, predictions obtained under the assumption of "constant" reptation time and inclusion of CR. The same figure includes, as dashed lines, model predictions using the average reptation time that the chains manifest at equilibrium, that is, dashed lines have been obtained using $\overline{\tau_{b,0}} = \sum w_i 3\tau_{e,0} Z_{eq,i}{}^3$, with PDI taken into account by the indirect method detailed above. (Of course, $\overline{\tau_{b,0}}$ speeds up as relaxation goes on due to CR.) Focusing on polymerization times up to 15 min, Figure 9 reveals that the experimental findings are better described by the equilibrium reptation dynamics rather than reptation in dilated tubes; in all cases, the predicted re-entanglement kinetics are faster than the actual kinetics. This feature also points to the direction of activated reptation dominating the re-entanglement dynamics of the samples obtained at these polymerization times.

As aforementioned, the idea of re-equilibration via means of reptation in dilated tubes seems to hold below a critical value of φ_e. Attention now shifts to the determination of this critical value. This is achieved using the results of Figures 6−9, that is, re-entanglement times for every sample are extracted from Figures 6−9 and are plotted as a function of φ_e. According to refs,[13,20] the time needed to reach 98% of the equilibrium value of the storage modulus can be defined as the re-entanglement (re-equilibration) time. (Method 1) An alternative approach is to fit the build-up data using eq 4, extract τ_b and β, and use the latter values in eq 5 to obtain the re-entanglement times. (Method 2) From a qualitative standpoint, results and corresponding conclusions do not depend on the employed method. To be consistent with refs,[13,20] results from Method 1 are discussed here. (Results from Method 2 can be found in Figure S25 of Section S7.) The experimental re-entanglement times are presented in Figure 10 as solid diamonds. Further, the re-entanglement times corresponding to the solid lines of Figures 7−9 are shown by unfilled diamonds. For comparison, Figure 10 also includes as cross symbols re-entanglement times corresponding to equilibrium reptation dynamics (see dashed lines of Figure 9). It also contains as open circles re-entanglement times referring to the entanglement recovery scenario at which the reptation time depends on $\Psi(t)$, that is, they refer to the dashed lines of Figure 8. Note that the experimental re-entanglement times of samples D4 and D5 were obtained using the second method since equilibration was not achieved within the experimental time window.

According to the upper panel of Figure 10, where re-entanglement times are plotted as a function of φ_e, the critical φ_e value is approximately 0.4. At larger φ_e values, especially above 0.5, the overall trend is that ordinary reptation in dilated tubes (in either version of eq 6a or eq 6b) severely underestimates the re-equilibration time. The $\varphi_e < 0.4$ regime comprises nine samples. There, the re-entanglement times referring to reptation in dilated tubes (unfilled diamonds and/or unfilled circles) compare well with the experimental results of six samples. The proposed approach underperforms for samples A3, B2, and D5. Focusing now on the two versions of the proposed molecular picture, that is, reptation independent of $\Psi(t)$ or reptation dependent on $\Psi(t)$, the latter version overall performs better in the $\varphi_e < 0.4$ regime; compared to unfilled diamonds, unfilled circles compare better with the experimental data (filled diamonds). Nevertheless, this version of the model assumes that newly created tube segments influence subsequent chain reorientation, a picture that contradicts the conventional picture of orientation relaxation in the tube theory.[6,7,25,26] The nonconventional picture could indeed be more realistic for UHMW chains because of the extremely long timescales needed for chain reorientation.

More likely, however, the conventional picture of relaxation is the correct one, and its underperformance, compared to the nonconventional picture, is related to the following two factors. First, moderate underestimation of the M_w and PDI values of samples C4, C5, D4, and D5. Recall that, for samples C4 and C5, SAOS data were not available, and hence the M_w and PDI values reported in ref 13 have been used. For the C3 sample for which SAOS data were available, slightly larger M_w and PDI values were found in this work. Further, the SAOS data of samples D4 and D5, used to infer the MWD, do not refer to a fully equilibrated state. As argued in Section 3, a fully entangled state would lead to higher M_w and PDI values. In this respect, all model predictions for samples C4, C5, D4, and D5 in Figure 10 would shift to longer re-entanglement times bringing the unfilled circles closer to the experimental data. Second, moderate variations in the initial state of the nascent melt are possible for materials obtained under the same conditions but belong to different groups. For example, samples C5 and D3 were obtained under the same polymerization conditions, including polymerization time. Further, they manifest the same φ_e value. Nevertheless, their re-entanglement times differ by a factor of 10. Likely, the initial state of the nascent melt of sample C5 is more heterogeneous than that of sample D3, meaning that entanglement homogenization represents the reality less appropriately for sample C5 than for sample D3. Recall that for the latter sample, filled and unfilled diamonds coincide.

The results shown in the upper panel of Figure 10 are re-presented in the bottom panel of the same figure as a function of M_w rather than φ_e. In terms of molecular weight, the critical value above which the proposed molecular picture appears to work is about 5000 kg/mol. The solid line represents the best fit to the data of refs,[13,20] as reported in the work of Pandey et al.[13] According to this line, the re-entanglement time scales with the power of 2.6 to the molecular weight. Further, the dashed line represents a best fit to the unfilled diamonds, that is, to the model predictions referring to reptation in a dilated tube under the assumption of $\Psi(t)$ independent reptation time. In this case, the re-entanglement time scales with the power of 3.7 to the molecular weight. In conclusion, homogenization of the initial entanglement density and subsequent entanglement reformation by means of chain reorientation via ordinary reptation in dilated tubes appear to work below a critical φ_e value that is approximately 0.4. For larger φ_e values, the actual re-entanglement process is dramatically longer than what the model suggests.

The severe underestimation of the re-entanglement time for short and intermediate polymerization times triggered the idea of allowing reorientation (and subsequently re-entanglement) to occur via CLF only. However, in this approach, the initial entanglement density was not homogenized along the whole chain length. In contrast, φ_e, the initial fraction of entangled melt, was equally distributed at the two chain extremities (see e.g., Figure 4—bottom right). Subsequently, the entangled fraction of the chain was allowed to renew orientation by means of CLF solely. In other words, reptation was suppressed in the model by setting the corresponding probability of eqs 7a and 7b to unity for all entangled chain segments. Figure S27 of Section S8 presents the results of this approach. It suggests that entanglement recovery via means of CLF solely is impossible since the elastic modulus builds up very slowly. For most cases, complete entanglement recovery is achieved far outside the experimental window. Even when re-entanglement is achieved within the experimental window, the shapes of the theoretical and experimental curves differ significantly. This finding also points in the direction of entanglement reformation via activated reptation when $\varphi_e > 0.4$.

The fact that reptation in a dilated tube was investigated as a plausible mechanism for re-entanglement might be surprising to the reader. This is because, even for the simpler system of shear-induced entanglement stripping, entanglement recovery is much slower than the equilibrium reorientation time.[49,50] Considering that the reorientation time for reptation in a dilated tube is always faster than the equilibrium reptation time, it would seem very unlikely that re-entanglement proceeds via reptation in a dilated tube. Indeed, the poor performance of the model is in accordance with the experimental findings of refs.[49,50] The reasons for which reptation in a dilated tube was considered are the following. First, unlike the shear-induced entanglement stripping case, the UHMW-PE chains experience deformations that are well within the linear viscoelastic regime. Thus, the chains do not stretch. The delayed re-entanglement time seen in refs[49,50] might arise from the waiting time for stretch relaxation before the onset of reptation and subsequent re-entanglement. Second, stress relaxation experiments on various UHMW-PE samples during the build-up, reported previously,[51] indicate that the reorientation time during the build-up is faster than the equilibrium reorientation time. At this point, it should be noted that these results are not in contradiction with the findings of Figures 3 and 10 (or Figure S25), that is, the experimental re-equilibration time is always considerably slower than the equilibrium reptation time (inverse of crossover frequency). This is because only the entangled sections of the chains are required to renew configuration for stress relaxation to occur.[24] This process is realized by means of nonactivated, partial reptation that does not require large scale diffusion of the whole chain, and thus it is faster than the bare reptation time.[24] In contrast, equilibration occurs via activated reptation, which is longer than the bare reptation time. In conclusion, the failure of the dilated tube model indicates that re-entanglement is an activated process. The better performance of the model at a low fraction of initial melt suggests that the activation barrier decreases with decreasing entanglement constraint. An activated reptation scenario, proposed by McLeish,[24] contains the aforementioned ingredients. For this reason, it is discussed in the following section, and its predictions are compared against the modulus build-up measurements.

4.3. Re-Entanglement Kinetics According to McLeish Theory.[24]

According to McLeish,[24] the confinement of the molten, disentangled sections is associated with an entropic penalty cost. This entropic cost drives the re-equilibration process of the metastable melt. However, re-entanglement itself is associated with a free energy cost too, since movement of the disentangled sections through the entangled domains causes deformation of the latter. Therefore, above a critical molecular weight, reptation occurs as an activated process. The free-energy barrier for this activated process reads

$$\Delta F_{\mathrm{bar}} = k_B T \left[A \left(\varphi_e \frac{N}{N_{e,\mathrm{eq}}} \right)^{2/3} - B N^{1/3} \right] \tag{13}$$

where A and B are order 1 factors, taken unity in ref 24, N is the degree of polymerization, and $N_{e,eq}$ is the entanglement degree of polymerization at equilibrium. In eq 13, φ_e is the initial fraction of the entangled melt, which can be determined from the experimental findings, that is, $\varphi_e = G_0/G_N^0$. It is to be noticed that the McLeish theory provides a prediction for φ_e. According to McLeish, this initial fraction of entangled melt is established via nonactivated, partial reptation, and it scales with Z_{eq} ($=N/N_{e,eq}$), the number of entanglements at equilibrium, according to $\varphi_e \approx Z_{eq}^{-1/3}$. The latter expression is compared against the experimentally determined φ_e values in Figure 11. There, a best fit to the data is provided by an expression of the form $\varphi_e \approx Z_{eq}^{-1/2.5}$, in reasonable agreement with McLeish's prediction.

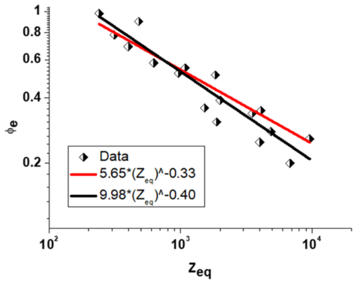

Figure 11. φ_e vs Z_{eq}. Symbols refer to experimental data, that is, $\varphi_e = G_0/G_N^0$. The red line refers to the prediction of McLeish while the black line is the best fit to the data.

The equilibration time reflecting activated reptation is derived from eq 13 leading to[24]

$$\tau = \tau_{b0}\ e^{\left[A\left(\varphi_e \frac{N}{N_{e,eq}}\right)^{2/3} - BN^{1/3}\right]} \tag{14}$$

with τ_{b0} being the unperturbed reptation time ($\tau_{b0} = 3\tau_{e,0}Z_{eq}^{3}$). These bare reptation times were estimated using the $\tau_{e,0}$ and $M_{e,eq}$ values obtained in Section 3, that is, $M_{e,eq} = 1250$ g/mol and $\tau_{e,eq} = 5 \times 10^{-8}$ s. The former values, together with the M_w values listed in Table 2, were used to determine the corresponding Z_{eq} values. Concerning the critical molecular weight, it is defined by $M_{w,crit} = M_0 N_{crit}$ where $N_{crit} = N_{e,eq}{}^2/\varphi_e{}^2$. Table 3 presents the φ_e and N_{crit} values for all examined samples. From Table 3, it becomes apparent that, for all samples of Table 2, M_w is well above the critical molecular weight. Hence, applicability of eq 14 is ensured. Using the φ_e values of Table 3, eq 14 has been incorporated to eq 3 producing the results shown in Figure 12 by dotted lines. Comparison of the latter curves with the experimental data reveals that the re-entanglement time is over-estimated. Notice that it is also impossible to match the experimental findings using eq 4 rather than eq 3 (Figure S28 of Section S9).

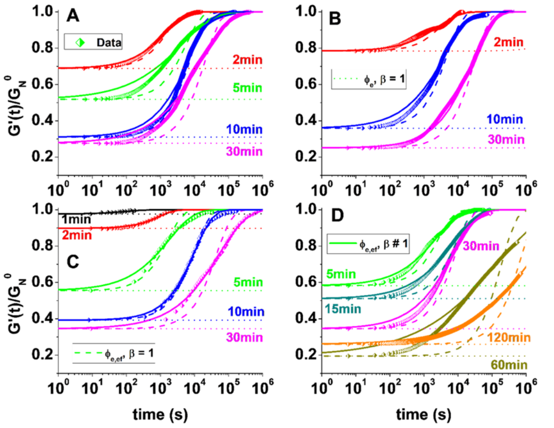

Figure 12. Comparison of the predictions of the McLeish theory[24] against the build-up measurements (symbols). Dotted lines correspond to theoretical predictions using the experimentally suggested φ_e values. Dashed lines are best fit to data (eqs 3 and 14) using effective values for φ_e. Solid lines are best fit to data (eqs 4 and 14) using effective values for φ_e and including PDI too. $T = 160$ °C, $M_{e,eq} = 1250$ g/mol, and $\tau_{e,eq} = 5 \times 10^{-8}$ s. MWD parameterization as well as φ_e and $\varphi_{e,ef}$ values are listed in Tables 2 and 3, respectively.

A decent fit to the build-up data is provided if lower φ_e values are allowed in eq 14 (but not in eqs 4 or 5—recall that $G_0 = \varphi_e G_N^0$.) Notice that the $\varphi_e N/N_{e,eq}$ term in eq 14 reflects the free energy cost associated with the movement of the disentangled sections through the entangled ones. In this respect, lower φ_e values translate to lower free-energy cost (more dilute entanglement network). Theoretical predictions using such reduced values for φ_e are presented in Figure 12 as solid and dashed lines. More specific, the dashed lines have been obtained by treating φ_e as the only fitting parameter, that is, PDI is disregarded. On the other hand, solid lines have been obtained when PDI is accounted for. In this case, eq 14 is substituted to eq 4 rather than to eq 3, with both φ_e and β being treated as fitting parameters. In both cases, the obtained effective values for φ_e are the same. These effective φ_e values, $\varphi_{e,ef}$, are listed in Table 3; on average, $\varphi_{e,ef}$ is diluted by a factor of 2 compared to the φ_e fraction suggested experimentally. The values for β can be found in Table S4 of Section S9.

The findings of Figure 12 suggest that the re-entanglement theory of McLeish[24] via activated reptation is qualitatively correct. From the perspective of quantitative agreement, the theory underperforms when the experimentally suggested values for φ_e are used, indicating that the free-energy cost for movement of the disentangled domains through the entangled ones is moderately lower than the one suggested by the theory. In other words, the entanglement mesh size of the entangled fraction of the melt, which needs to be deformed as

Table 3. Initial fraction of Entangled Melt as Suggested Experimentally and the Effective fraction Needed to Capture the Build Data for Every Sample of Groups A to D[a]

samples	φ_e	$\varphi_{e,ef}$	N_{crit}	$M_{w,crit} = N_{crit}M_0$ kg/mol
group A: A1, A2, A3, A4	0.69, 0.52, 0.31, 0.28	0.43, 0.25, 0.16, 0.09	4188, 7389, 20 590, 25 990	117.5, 207.3, 577.6, 729.0
group B: B1, B2, B3	0.78, 0.36, 0.25	0.54, 0.18, 0.11	3230, 15 409, 31 471	90.6, 432.2, 882.8
group C: C1, C2, C3, C4, C5	0.98, 0.90, 0.55, 0.39, 0.35	0.55, 0.37, 0.22, 0.16, 0.11	2082, 2462, 6448, 12 900, 16 667	58.4, 69.1, 180.9, 361.8, 467.5
group D: D1, D2, D3, D4, D5	0.58, 0.51, 0.34, 0.20, 0.26	0.32, 0.17, 0.11, 0.08, 0.07	5866, 7626, 16 710, 29 488, 52 390,	164.6, 213.9, 468.7, 1469.5, 827.13

[a] The table also lists the critical degree of polymerization and the corresponding molecular weight above which eq 14 is valid.

DOI: 10.1021/acs.macromol.9b01152
Macromolecules 2019, 52, 8849−8866

for the disentangled domains to move, appears to be more dilute than originally suggested. In the limit of considerably low φ_e, the effective entanglement network influencing the motion of the disentangled domains is so dilute that re-entanglement can be described by ordinary reptation in dilated tubes even if the initial entanglement density is homogenized (Section 4.2).

An alternative explanation could be that the factors A and B appearing in eq 13 are not unity but slightly different. To examine this possibility, various combinations of A and B were considered, and the predictions of eq 14 were compared against the build-up data. In this process, the experimentally suggested φ_e values were used, and PDI was allowed, that is, eq 14 was incorporated to eq 4. Combinations for which $A \approx B/2$ give predictions that compare well with the data. In particular, the combinations $A = 0.25$ and $B = 0.5$, $A = 0.5$ and $B = 1.0$, and $A = 0.75$ and $B = 1.5$ give the best predictions among all examined combinations. Further, the build-up data of each sample was fitted using eqs 4 and 14 with A and B treated as fitting parameters. Figure 13 below and Figure S29 of Section S9 present good fits of the data. In the former case, $A = 0.6 \pm 0.15$ and $B = 1 \pm 0.1$, whereas in the latter case, $A = 0.3 \pm 0.15$ and $B = 0.5 \pm 0.1$. The exact values of A, B, and β for each sample can be found in Tables S5 and S6 of Section S9. From Figures 13 and S29, it becomes apparent that the activated reptation theory of McLeish can provide a good description of the data, provided that the constant in the elastic energy term is about half the constant in the confinement energy term, that is, $A \approx B/2$ in eqs 13 and 14. Overall, the good comparison between theory and data lends strong support to the notion of equilibration through activated reptation.

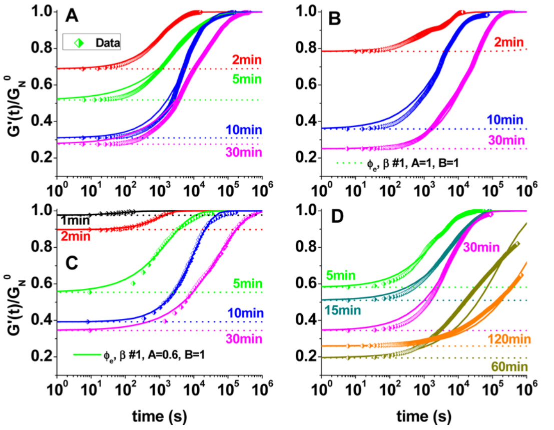

Figure 13. Predictions of the McLeish theory (lines) and build-up data (symbols). Dotted and solid lines refer, respectively, to $A = B = 1$ and $A \approx 0.6$, $B \approx 1$ (see eqs 13 and 14). φ_e values used are those suggested experimentally, that is, $\varphi_e = G_0/G_N^0$.

5. RHEOLOGY OF EQUILIBRATED AND NONEQUILIBRATED UHMW-PE USING ALTERNATIVE TUBE MODEL PARAMETERIZATION

The tube model parameterization used in the previous sections was established considering the SAOS data of the UHMW-PE samples A1, C3, and D1 (see Sections 2 and S4). The values of this parameterization set are $G_N^0 = 2.2$ MPa, $M_{e,eq} = 1250$ g/mol, and $\tau_{e,eq} = 5 \times 10^{-8}$ s at 160 °C (parameterization I). Nevertheless, the actual MWD of the aforementioned samples is unknown. For this reason, it has been suggested by one of the reviewers of this manuscript that the tube model parameters should be determined by matching model predictions with the SAOS data of polymer melts that have their MWD determined experimentally. Regarding non-UHMW-PE linear chains, GPC traces are available for three PE materials, namely the HDL2, HDL3, and HDL4 grades.[17] HDL stands for High Density Linear (topology). Concerning UHMW-PE chains, GPC traces are available for one grade.[20,21] According to the GPC results of refs,[20,21] the M_w and PDI of this grade are 2370 kg/mol and 1.2, respectively. Nevertheless, these M_w and PDI values are questionable since homogeneous dissolution of chains exceeding 2×10^6 g/mol in common organic solvents is cumbersome.[20,21] For this reason, it was decided to use the GPC traces of the HDL grades to determine the values of the tube model parameters. Further, it was decided to retain the same values for G_N^0 and $M_{e,eq}$ as in parameterization I, that is, $G_N^0 = 2.2$ MPa and $M_{e,eq} = 1250$ g/mol. The reason for keeping the same values is twofold. First, the aforementioned values lie within the range of values reported in the literature.[17,18,25,26,36,41] Second, chain dynamics are more sensitive to small changes of $\tau_{e,eq}$ rather than to small changes of G_N^0.

Figure 14A presents the comparison between the TMA predictions and the SAOS data of the HDL series. The molecular characteristics of the HDL grades can be found in Table S1. Since the GPC traces of those samples are experimentally known, the only fitting parameter here is the entanglement relaxation time, $\tau_{e,eq}$. The best fit to the SAOS data corresponds to $\tau_{e,eq} = 9 \times 10^{-9}$ s. Note that the latter value refers to 150 °C, the temperature at which the rheology measurements on the HDL materials were performed. The $\tau_{e,eq}$ (150 °C) value was shifted to various temperatures using an activation energy of 29.14 kJ/mol. This activation energy corresponds to an average value of activation energies found in the literature for high-density PEs, linear low-density PEs, and linear homopolymer PE chains (see Section S5). Notice that activation energies for low-density PEs (LDPEs) were excluded when estimating the aforementioned average value.

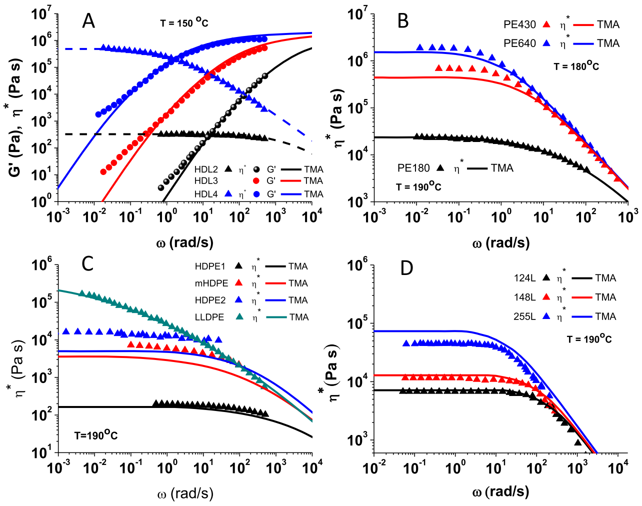

Figure 14. Comparison of SAOS data (symbols) and TMA predictions for several entangled PE melts comprising non-UHMW chains using parameterization II. The molecular characteristics of the grades are reported in Tables S1 and S2. The data are reproduced from refs.[17,18,36,41,42]

This is because LDPEs contain long side-chain branches that might affect the entanglement relaxation time.

Figure 14B−D compares the TMA predictions and SAOS data of various non-UHMW-PE grades using the shifted $\tau_{e,eq}$ values, in particular, $\tau_{e,eq} = 7.4 \times 10^{-9}$ s at 160 °C, $\tau_{e,eq} = 5.2 \times 10^{-9}$ s at 180 °C, and $\tau_{e,eq} = 4.4 \times 10^{-9}$ s at 190 °C. The molecular characteristics of the non-UHMW grades are reported in Tables S1 and S2. Rather than the complete GPC traces, experimentally determined M_w and PDI values were only available for those grades.[18,36,41,42] Therefore, their MWD was constructed assuming a log-normal distribution. Overall, the comparison between the TMA predictions and the SAOS measurements presented in Figure 14B−D is good. Notice that the fitting using the new parameterization is significantly better than the fitting using the $\tau_{e,eq}$ value of the previous parameterization (see Figure S20 of the Supporting Information).

Next, the M_w and PDI values for the UHMW-PE materials reported in Table 1 were estimated using the new parameterization, that is, $G_N^0 = 2.2$ MPa, $M_{e,eq} = 1250$ g/mol, and $\tau_{e,eq} = 7.4 \times 10^{-9}$ s at 160 °C (parameterization II). To recall, log-normal distributions are considered in constructing the MWDs of the materials. Figure 15 shows the best fits to the SAOS data of samples A1 to D5. The extracted M_w and PDI values are reported in Table 4. Compared to Table 2, which reports M_w and PDI values using parameterization II, the M_w values are approximately doubled. In contrast, the PDI values are similar since changes in $\tau_{e,eq}$ correspond to a horizontal shift of the predicted curves, leaving their shape unchanged. The longest molecular weight found is 21.5 million g/mol that seems rather unrealistic. An explanation of this peculiar result could be that the entanglement relaxation time of UHMW chains differs from that of non-UHMW linear chains. For a given temperature, there could be a critical M_w above which $\tau_{e,eq}$ slows down compared to $\tau_{e,eq}$ below the critical molecular weight.

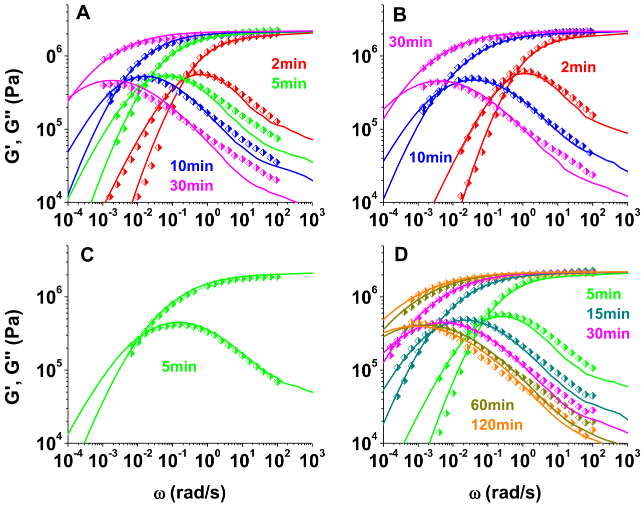

Figure 15. Same as Figure 3 using parameterization II. The obtained M_w and PDI values are listed in Table 4.

To examine this scenario further, TMA predictions obtained using parameterization II and the GPC trace of the UHMW-PE grade found in refs[20,21] were compared against the experimental observations. The comparison can be seen in Figure 16A where symbols refer to SAOS data while black lines are model predictions. As readily seen from Figure 16A, the tube model under-predicts the terminal relaxation. This discrepancy supports the scenario of $\tau_{e,eq}$ being slower for UHMW chains. Another plausible scenario however is that the GPC trace is not completely accurate, that is, the high-molecular-weight tail of the distribution is not determined precisely by GPC. This scenario cannot be excluded.

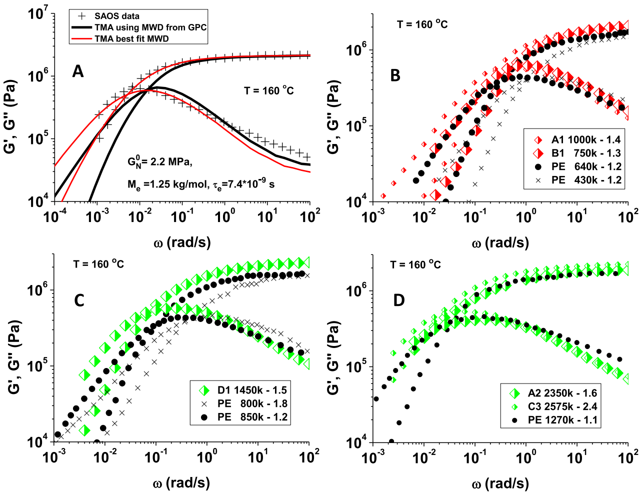

Figure 16. (A) SAOS curves of UHMW-PE having M_w about 2×10^6 g/mol. In obtaining theoretical prediction, the GPC determined MWD has been used. (B−D) Comparison of SAOS data of the materials A1, A2, B1, C3, and D5 (Table 4) and of the PE series of refs.[18,42]

Figure 16B−D compares the equilibrium SAOS data of samples A1, A2, B1, C3, and D1 with the SAOS data of entangled PE samples that are supposed to have comparable molecular weights. In more detail, the M_w (PDI) values of these samples are 430 kg/mol (1.2), 640 kg/mol (1.2), 800 kg/mol (1.8), 850 kg/mol (1.2), and 1270 (1.1). These values have been obtained through GPC.[18,42] Nevertheless, the exact GPC traces are unavailable. It is to be noticed that the SAOS measurements of grades PE430, PE640, PE800, PE850, and PE1270 were carried out at temperatures other than 160 °C,

Table 4. Same as Table 2 Using Parameterization II

samples	polymerization time (minutes)	M_w kg/mol	PDI index
group A: A1, A2, A3, A4	2, 5, 10, 30	1000, 2350, 4100, 11 400 (700, 1200, 2300, 5600)	1.4, 1.6, 1.7, 2.4 (1.3, 2, 1.9, 3.2)
group B: B1, B2, B3	2, 10, 30	750, 3800, 8950 (600, 1800, 4200)	1.3, 2.2, 2.5 (1.2, 1.8, 2.4)
group C: C1, C2, C3, C4, C5	1, 2, 5, 10, 30	-, -, 2575, -, - (300, 600, 1400, 2500, 5100)	-, -, 2.4, -, - (1.4, 1.7, 2.5, 2.4, 2.5)
group D: D1, D2, D3, D4, D5	5, 15, 30, 60, 120	1450, 4450, 8800, 16 250, 21 500 (970, 2370, 4190, 5630, 7110)	1.5, 2.1, 2.7, 3.5, 4.0 (1.8, 2.4, 2.5, 3.2, 3.0)

DOI: 10.1021/acs.macromol.9b01152
Macromolecules 2019, 52, 8849−8866

where the SAOS response of the A1, A2, B1, C3, and D1 grades was measured. Thus, the dynamic moduli of the former grades were shifted to 160 °C using the effective set of a_T and b_T shift factors determined in Section S5. In more detail, the a_T values were obtained considering the average activation energy of 29.14 kJ/mol. The comparison shown in Figure 16B,C seems reasonable. For example, the PE640 data lie close to the data of the B1 sample, which is found to have M_w = 750 kg/mol. Further, the cross-over frequency of the D1 sample (1450 kg/mol—PDI 1.5) is positioned about one decade lower than the cross-over frequency of the PE800 sample. On the other hand, the small separation between the PE1270 data and the A2/C3 data raises concerns since the A2 and C3 samples are supposed to comprise chains that are twice as long as those in the PE1270 material. The analogous figures of Figure 16B–D are Figures S22 and S23; here, parameterization I is utilized in the SAOS data fitting.

Shifting attention to the modulus build-up data (re-entanglement process), Figure 17 presents the analogous figure of Figure 8, that is, model predictions for re-entanglement via ordinary reptation in dilated tubes are compared against the actual build-up measurements. Rather than parameterization I and the M_w/PDI values of Table 2, parameterization II and the M_w/PDI values of Table 4 are utilized in obtaining the theoretical predictions. Concerning the grades for which SAOS data are not available, that is, C1–C2 and C4–C5, the M_w values were approximately doubled compared to the values reported in ref 13. With respect to the PDI values, these were taken from Pandey et al.[13] These choices were based on our findings for the C3 grade for which SAOS data is available, that is, the extracted M_w value is 1.8 times larger than the one reported by Pandey et al., whereas the PDI value is very close to the one reported by the same authors. TMA predictions shown in Figure 17 are obtained in the presence of CR, using "constant" and time-dependent reptation times in accordance with eqs 6a and 6b, respectively. Solid lines refer to the former scenario, whereas dashed lines refer to the latter scenario. It is to be noticed that the theoretical results of Figures 8 and 17 are very similar. This feature is not surprising since the speed up of the entanglement relaxation time is compensated by the increase in the molecular weight of the chains. Moreover, similar to Figure 8, the theory performs better with increasing molecular weight (decreasing φ_e). The reasons for this behavior are detailed in Section 4.

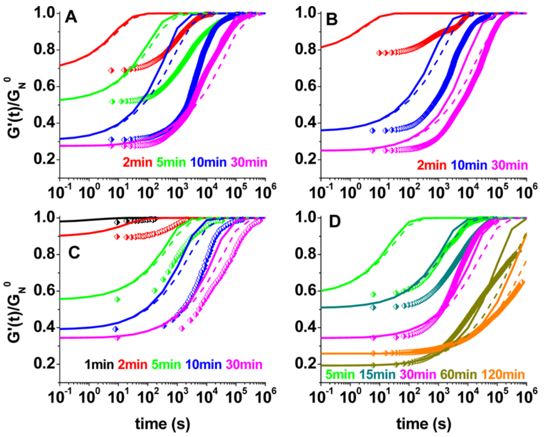

Figure 17. Comparison of model outcomes (eq 12—lines) and build-up measurements (symbols) for the samples of groups A to D. Subreptative modes are included as well as CR. PDI is treated using the indirect approach. Dashed and solid lines correspond to time-dependent and "constant" reptation times, respectively. $M_{e,eq}$ = 1250 g/mol and $\tau_{e,eq} = 7.4 \times 10^{-9}$ s.

The better performance of the ordinary, nonactivated reptation model with increasing M_w (decreasing φ_e) can also be seen in Figure 18. In the latter figure, model predictions refer to nonactivated reptation either in dilated or equilibrated tubes. Similar to Figure 10, theoretical predictions, in either version of the model, better compare to experimental re-entanglement times below a threshold φ_e value, which is about 0.4–0.5. In terms of molecular weight, this threshold value is 4000 kg/mol approximately. According to the findings of Section 4, for φ_e values above the threshold value, re-orientation and in turn re-entanglement occur via activated reptation.

Quantitative analysis of this activated reptation process was carried out in Section 4.3 utilizing the theory of McLeish.[24] Below, this analysis is repeated using parameterization II rather than parameterization I. In more detail, Figure 19 displays φ_e as a function of Z_{eq}. According to McLeish, φ_e scales with Z_{eq} according to $\varphi_e \approx Z_{eq}^{-1/3}$ (red line). Since M_w values for all samples are doubled when parameterization II is used, the data (symbols) are better described by an expression of the form $\varphi_e \approx Z_{eq}^{-1/2.5}$ (black line) similar to Figure 11.

Further, the analysis performed in Section 4.3 revealed that the activated reptation theory of McLeish[24] can provide a quantitative description of the build-up data, provided that the magnitude of the (elastic deformation) free energy barrier is lower than in the original theory. This elastic deformation barrier can be lowered either by assuming effective values for φ_e or by adjusting the relative strength between the elastic deformation barrier and the confinement barrier (through the prefactors A and B appearing in eq 13). Figure 20 displays the

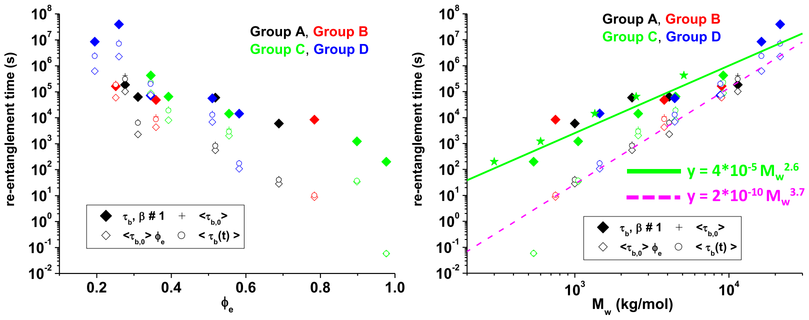

Figure 18. Same as Figure 10 using parameterization II and the M_w/PDI values listed in Table 4.

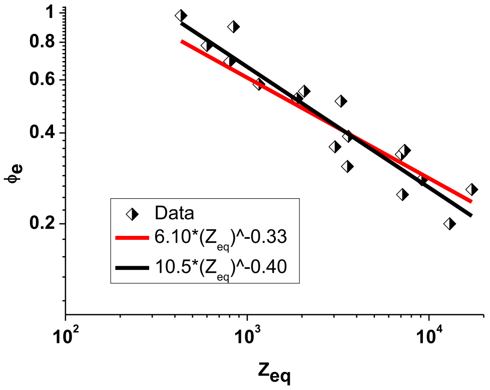

Figure 19. φ_e vs Z_{eq} using parameterization II. Symbols refer to data, that is, $\varphi_e = G_0/G_N^0$. The red line refers to the prediction of McLeish while the black line is the best fit to the data.

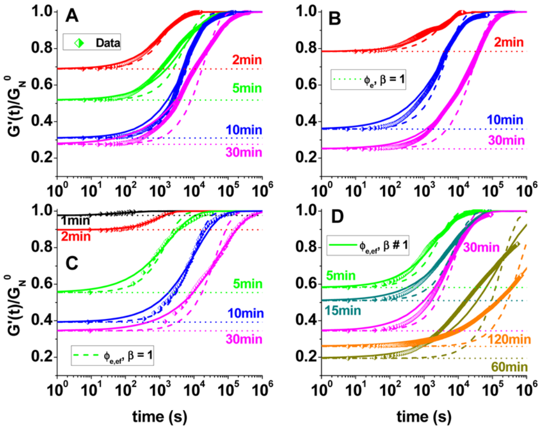

Figure 20. Same comparison of the predictions of the McLeish theory against the build-up measurements as Figure 12 using parameterization II. φ_e values are reported in the first column of Table 3. M_w values are reported in Table 4. $\varphi_{e,ef}$ and β values are listed in the first and second columns of Table 5, respectively.

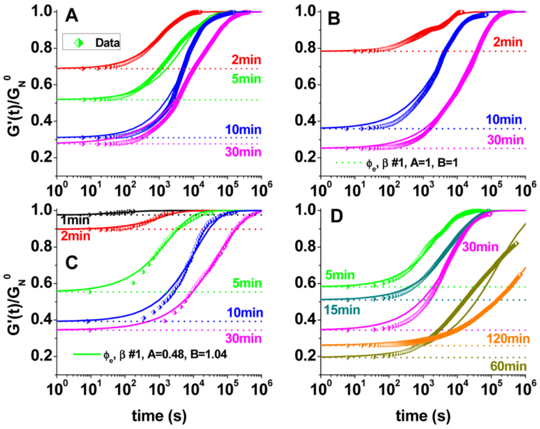

Figure 21. Same as Figure 13 using parameterization II and the M_w values reported in Table 4.

comparison between predictions and measurements when the first option is considered. It is the analogous figure of Figure 12. It has been obtained using parameterization set II. The $\varphi_{e,ef}$ and β values extracted from the fits are reported in the first two columns of Table 5. The effective φ_e values are moderately lower than those reported in Table 3 because the molecular weights, and in turn the equilibrium number of entanglements, are larger. The β values differ occasionally from those listed in Table S4 in an attempt to impose a better correlation between β and the PDI values reported in Table 4. Figure 21 is the analogous figure of Figure 13. φ_e values used are those suggested experimentally. Here, the deformation barrier is lowered by adjusting the A and B prefactors of eq 13. Considering the same β values as above, the best fits to the data are provided when $A \approx B/2$, similar to Figure 13. However, the average value of A is somewhat lower than in Figure 13 since the molecular weights extracted from parameterization II are higher than those inferred from parameterization I. The exact A and B values obtained from the fits shown in Figure 21 are listed in the last two columns of Table 5.

In conclusion, this section demonstrated that the main findings of this manuscript are insensitive to moderate changes in the tube model parameterization, that is, the findings of this work indicate that re-entanglements occur via activated reptation, a process that takes longer than ordinary diffusion in dilated or equilibrated tubes. As φ_e decreases, the activated reptation time speeds up, becoming comparable to the equilibrium reptation time of the chains.

6. CONCLUSIONS

The main purpose of this work was to contribute to the molecular understanding of the equilibrium and nonequilibrium dynamics of polymer melts of linear, UHMW-PE chains. Concerning the equilibrium dynamics, that is, chain reorientation in melts of homogeneous entanglement density, it was found that dynamic moduli data can be captured by typical tube models. Therefore, the MWD of several UHMW-PE samples was determined using ordinary, nonactivated reptation. A unique parameterization set was used for the tube model parameters, namely, the entanglement molecular weight, the entanglement plateau modulus, and the entanglement relaxation time. The inferred M_w and PDI values are very sensitive to changes in the tube model parameters, especially the entanglement relaxation time. From a quantitative standpoint, further theoretical as well as experimental efforts are required to infer the MWD of UHMW-PE chains with higher accuracy. Specifically, it would be desirable to have

Table 5. For Every Sample of Groups A to D, Effective φ_e and β Values Required to Fit the Build-Up Data Using the McLeish Model (Figure 20)[a]

samples	$\varphi_{e,ef}$	β	A	B
group A: A1, A2, A3, A4	0.29, 0.17, 0.12, 0.07	0.73, 0.67, 0.70, 0.53	0.54, 0.49, 0.53, 0.46	0.96, 1.02, 0.98, 1.15
group B: B1, B2, B3	0.36, 0.13, 0.08	0.70, 0.62, 0.60	0.56, 0.50, 0.46	0.93, 0.99, 0.98
group C: C1, C2, C3, C4, C5	0.40, 0.27, 0.16, 0.12, 0.08	0.73, 0.70, 0.61, 0.63, 0.55	0.53, 0.47, 0.47, 0.48,0.43	0.97, 1.04, 1.09, 1.07, 1.16
group D: D1, D2, D3, D4, D5	0.23, 0.12, 0.08, 0.06, 0.05	0.68, 0.62, 0.60, 0.48, 0.40	0.53, 0.41, 0.41, 0.47, 0.37	0.97, 1.09, 1.09, 1.03, 1.07

[a] The table also lists the A and B values obtained from the fits presented in Figure 21.

GPC traces of various PE melts having low and intermediate molecular weights, that is, up to 1500−2000 kg/mol. It would also be desirable to complement GPC data with SAOS and creep measurements at various melt temperatures (with the aim to construct master curves and establish shift factors). Such experimental information, together with SAOS measurements on even higher molecular weights, would provide crucial input to theoretical efforts focusing on elucidating whether the SR-activated reptation model is superior to the ordinary reptation model in describing the SAOS response of UHMW-PE. It would also assist to clarify whether the entanglement relaxation time changes above a critical molecular weight.

As regards the nonequilibrium dynamics, that is, the entanglement recovery occurring in the metastable (heterogeneous) melt, a tube model-based approach was introduced and tested against the build-up data. This approach homogenizes the initial entangled fraction of the melt and confines the chains into dilated tubes, that is, to tubes with larger diameter than that at equilibrium, taking into account their partially entangled nature. Re-entanglement is viewed as the complementary process of chain reorientation. The latter occurs as chains reptate out of the dilated tubes. The introduced framework readily accommodates second-order effects such as PDI, CR, CLF, and subreptative modes. CLF has a small influence on the (reorientation) re-entanglement dynamics, as expected for UHMW chains. CR accelerates the re-entanglement dynamics moderately. With respect to PDI, a direct treatment misjudges the re-equilibration time because the model severely underestimates the reorientation time of the shorter chains of the MWD. In contrast, the model performs better with increasing molecular weight. The longer the chain, the lower the initial fraction of entangled melt, and therefore, the homogenization of the latter quantity (φ_e) becomes more realistic. In this respect, the model performs reasonably well below a threshold value of 0.4.

Above the threshold value, the proposed approach performs poorly as it harshly underestimates the re-entanglement time of the chains. Since the experimentally determined re-entanglement times are significantly longer than the equilibrium reptation times, it appears that reorientation occurs via an activated reptation process in line with the model of McLeish.[24] Here, movement of disentangled chain sections through the entangled fraction of the melt is associated with an elastic free-energy cost. The latter depends on the quantity $\varphi_e N/N_{e,eq}$.[24] Nevertheless, to match the modulus build-up data, the magnitude of the (elastic) free energy barrier has to be lowered compared to the original theory, suggesting that during their reorientation, the chains experience less confinement from their surroundings than that assumed by the original McLeish theory. It is to be noticed that the activated reptation picture holds both above and below the threshold value of φ_e. Nevertheless, in the low φ_e limit, the free-energy cost is low enough so that the actual re-entanglement times become comparable to the equilibrium, nonactivated reptation times. In some occasions, that is, for some samples, the re-entanglement times speed up so drastically that become even comparable to the re-orientation times associated with reptation in dilated tubes.

■ ASSOCIATED CONTENT

Ⓢ Supporting Information

The Supporting Information is available free of charge on the ACS Publications website at DOI: 10.1021/acs.macromol.9b01152.

> Additional information on the reliability of the modulus build-up data, information on the activated reptation theory of Semenov and Rubinstein and its comparison to the usual tube theory, comparison of the predictions of different tube model implementations for UHMW-PE, information on the tube model parameterization used for the MWD determination of the equilibrated samples, reliability of the adopted tube model parameterization by comparing model predictions against SAOS data on non-UHMW-PE melts, comparison of MWDs determined by GPC and rheology (tube model), details of the calculation of re-entanglement times from the build-up data, effect of CLFs, information regarding the performance of the re-entanglement model of McLeish, and Rouse model and reptation in dilated tubes (PDF)

■ AUTHOR INFORMATION

Corresponding Author

*E-mail: laurence.hawke@maastrichtuniversity.nl.

ORCID

Laurence G. D. Hawke: 0000-0001-7975-7820

Sanjay Rastogi: 0000-0002-7804-7349

Notes

The authors declare no competing financial interest.

■ ACKNOWLEDGMENTS

The authors would like to acknowledge Prof. D. Vlassopoulos (FORTH, Univ. of Crete) and Prof. N. Grizzuti (UNINA, Univ. of Naples Federico II) for fruitful discussions and suggestions.

■ REFERENCES

(1) Rastogi, S.; Yao, Y.; Ronca, S.; Bos, J.; van der Eem, J. Unprecedented High-Modulus High-Strength Tapes and Films of Ultrahigh Molecular Weight Polyethylene via Solvent-Free Route. *Macromolecules* **2011**, *44*, 5558−5568.

(2) Romano, D.; Tops, N.; Andablo-Reyes, E.; Ronca, S.; Rastogi, S. Influence of Polymerization Conditions on Melting Kinetics of Low Entangled UHMWPE and Its Implications on Mechanical Properties. *Macromolecules* **2014**, *47*, 4750−4760.

(3) Ronca, S.; Forte, G.; Tjaden, H.; Rastogi, S. Solvent-Free Solid-State-Processed Tapes of Ultrahigh-Molecular-Weight Polyethylene: Influence of Molar Mass and Molar Mass Distribution on the Tensile Properties. *Ind. Eng. Chem. Res.* **2015**, *54*, 7373−7381.

(4) Romano, D.; Tops, N.; Bos, J.; Rastogi, S. Correlation between Thermal and Mechanical Response of Nascent Semicrystalline UHMWPEs. *Macromolecules* **2017**, *50*, 2033−2042.

(5) Marissen, R. Design with Ultra Strong Polyethylene Fibers. *Mater. Sci. Appl.* **2011**, *02*, 319−330.

(6) Likhtman, A. E.; McLeish, T. C. B. Quantitative Theory for Linear Dynamics of Linear Entangled Polymers. *Macromolecules* **2002**, *35*, 6332−6343.

(7) McLeish, T. C. B. Tube theory of entangled polymer dynamics. *Adv. Phys.* **2002**, *51*, 1379−1527.

(8) Smith, P.; Lemstra, P. J. Ultrahigh-strength polyethylene filaments by solution spinning/drawing, 2. Influence of solvent on the drawability. *Macromol. Chem.* **1979**, *180*, 2983−2986.

(9) Smith, P.; Lemstra, P. J. Ultra-high-strength polyethylene filaments by solution spinning/drawing. *J. Mater. Sci.* **1980**, *15*, 505−514.

(10) Rastogi, S.; Lippits, D. R.; Peters, G. W. M.; Graf, R.; Yao, Y.; Spiess, H. W. Heterogeneity in polymer melts from melting of polymer crystals. *Nat. Mater.* **2005**, *4*, 635−641.

(11) Lippits, D. R.; Rastogi, S.; Talebi, S.; Bailly, C. Formation of Entanglements in Initially Disentangled Polymer Melts. *Macromolecules* **2006**, *39*, 8882−8885.

(12) Choudhary, S. *Solid State Deformation of Disentangled Ultra High Molecular Weight Polyethylene; Influence of Molecular Weight on Mechanical Properties*; Eindhoven University of Technology, 2011.

(13) Pandey, A.; Champouret, Y.; Rastogi, S. Heterogeneity in the Distribution of Entanglement Density during Polymerization in Disentangled Ultrahigh Molecular Weight Polyethylene. *Macromolecules* **2011**, *44*, 4952−4960.

(14) Romano, D.; Andablo-Reyes, E. A.; Ronca, S.; Rastogi, S. Effect of a cocatalyst modifier in the synthesis of ultrahigh molecular weight polyethylene having reduced number of entanglements. *J. Polym. Sci., Part A: Polym. Chem.* **2013**, *51*, 1630−1635.

(15) Pandey, A.; Toda, A.; Rastogi, S. Influence of Amorphous Component on Melting of Semicrystalline Polymers. *Macromolecules* **2011**, *44*, 8042−8055.

(16) Liu, K.; de Boer, E. L.; Romano, D.; Ronca, S.; Ronca, S.; Rastogi, S. Heterogeneous Distribution of Entanglements in a Nonequilibrium Polymer Melt of UHMWPE: Influence on Crystallization without and with Graphene Oxide. *Macromolecules* **2016**, *49*, 7497−7509.

(17) Wood-Adams, P. M.; Dealy, J. M.; deGroot, A. W.; Redwine, O. D. Effect of Molecular Structure on the Linear Viscoelastic Behavior of Polyethylene. *Macromolecules* **2000**, *33*, 7489−7499.

(18) Vega, J. F.; Rastogi, S.; Peters, G. W. M.; Meijer, H. E. H. Rheology and reptation of linear polymers. Ultrahigh molecular weight chain dynamics in the melt. *J. Rheol.* **2004**, *48*, 663−678.

(19) Mead, D. W. Determination of molecular weight distributions of linear flexible polymers from linear viscoelastic material functions. *J. Rheol.* **1994**, *38*, 1797−1827.

(20) Talebi, S. *Disentangled Polyethylene with Sharp Molar Mass Distribution: Implications for Sintering*; Eindhoven University of Technology, 2008.

(21) Talebi, S.; Duchateau, R.; Rastogi, S.; Kaschta, J.; Peters, G. W. M.; Lemstra, P. J. Molar Mass and Molecular Weight Distribution Determination Of UHMWPE Synthesized Using a Living Homogeneous Catalyst. *Macromolecules* **2010**, *43*, 2780−2788.

(22) Semenov, A. N.; Rubinstein, M. Dynamics of strongly entangled polymer systems: activated reptation. *Eur. Phys. J. B* **1998**, *1*, 87−94.

(23) Vettorel, T.; Kremer, K. Development of Entanglements in a Fully Disentangled Polymer Melt. *Macromol. Theory Simul.* **2010**, *19*, 44−56.

(24) McLeish, T. C. B. A theory for heterogeneous states of polymer melts produced by single chain crystal melting. *Soft Matter* **2007**, *3*, 83−87.

(25) van Ruymbeke, E.; Keunings, R.; Bailly, C. Prediction of linear viscoelastic properties for polydisperse mixtures of entangled star and linear polymers: Modified tube-based model and comparison with experimental results. *J. Non-Newtonian Fluid Mech.* **2005**, *128*, 7−22.

(26) Das, C.; Inkson, N. J.; Read, D. J.; Kelmanson, M. A.; McLeish, T. C. B. Computational linear rheology of general branch-on-branch polymers. *J. Rheol.* **2006**, *50*, 207−234.

(27) Kontopoulou, M.; Vlachopoulos, J. Bubble Dissolution in Molten Polymers and Its Role in Rotational Molding. *Polym. Eng. Sci.* **1999**, *39*, 1189−1198.

(28) Deplancke, T.; Lame, O.; Rousset, F.; Aguili, I.; Seguela, R.; Vigier, G. Diffusion versus Cocrystallization of Very Long Polymer Chains at Interfaces: Experimental Study of Sintering of UHMWPE Nascent Powder. *Macromolecules* **2013**, *47*, 197−207.

(29) Rastogi, S.; Kurelec, L.; Lippits, D.; Cuijpers, J.; Wimmer, M.; Lemstra, P. J. Novel Route to Fatigue-Resistant Fully Sintered Ultrahigh Molecular Weight Polyethylene for Knee Prosthesis. *Biomacromolecules* **2005**, *6*, 942−947.

(30) de Boer, E. L. *Implications of a Tailored Non-equilibrium Polymer Melt State on the Viscoelastic Response and Crystallisation Behaviour of UHMWPE*; Loughborough University, 2016.

(31) Bates, F. S.; Wignall, G. D.; Koehler, W. C. Critical Behavior of Binary Liquid Mixtures of Deuterated and Protonated Polymers. *Phys. Rev. Lett.* **1985**, *55*, 2425−2428.

(32) Bates, F. S.; Fetters, L. J.; Wignall, G. D. Thermodynamics of Isotopic Polymer Mixtures: Poly(vinylethylene) and Poly(ethylethylene). *Macromolecules* **1988**, *21*, 1086−1094.

(33) Liu, K.; Ronca, S.; Andablo-Reyes, E.; Forte, G.; Rastogi, S. Unique Rheological Response of Ultrahigh Molecular Weight Polyethylenes in the Presence of Reduced Graphene Oxide. *Macromolecules* **2015**, *48*, 131−139.

(34) Lippits, D. R.; Rastogi, S.; Höhne, G. W. H. Melting Kinetics in Polymers. *Phys. Rev. Lett.* **2006**, *96*, 218303.

(35) Lippits, D. R.; Rastogi, S.; Höhne, G. W. H.; Mezari, B.; Magusin, P. C. M. M. Heterogeneous Distribution of Entanglements in the Polymer Melt and Its Influence on Crystallization. *Macromolecules* **2007**, *40*, 1004−1010.

(36) Pattamaprom, C.; Larson, R. G. Predicting the linear viscoelastic properties of monodisperse and polydisperse polystyrenes and polyethylenes. *Rheol. Acta* **2001**, *40*, 516−532.

(37) Hamad, F. G.; Colby, R. H.; Milner, S. T. Onset of Flow-Induced Crystallization Kinetics of Highly Isotactic Polypropylene. *Macromolecules* **2015**, *48*, 3725−3738.

(38) Wilsens, C. H. R. M.; Hawke, L. G. D.; Troisi, E. M.; Hermida-Merino, D.; de Kort, G.; Saralidze, K.; Peters, G. W. M.; Rastogi, S.; Rastogi, S. Effect of self-assembly of oxalamide based organic compounds on melt behavior, nucleation, and crystallization of isotactic polypropylene. *Macromolecules* **2018**, *51*, 4882−4895.

(39) Wilsens, C. H. R. M.; Hawke, L. G. D.; de Kort, G. W.; Saidi, M.; Leoné, N.; Hermida-Merino, D.; Peters, G. W. M.; Rastogi, S.; Rastogi, S. Effect of Thermal History and Shear on the Viscoelastic Response of iPP Containing an Oxalamide-Based Organic Compound. *Macromolecules* **2019**, *52*, 2789−2802.

(40) Milner, S. T.; McLeish, T. C. B. Reptation and Contour-Length Fluctuations in Melts of Linear Polymers. *Phys. Rev. Lett.* **1998**, *81*, 725−728.

(41) Lohse, D. J.; Milner, S. T.; Fetters, L. J.; Xenidou, M.; Hadjichristidis, N.; Mendelson, R. A.; García-Franco, C. A.; Lyon, M. K. Well-Defined, Model Long Chain Branched Polyethylene. 2. Melt Rheological Behavior. *Macromolecules* **2002**, *35*, 3066−3075.

(42) Lippits, D. R. *Controlling the Melting Kinetics of Polymers; a Route to a New Melt State*; Eindhoven University of Technology, 2007.

(43) Hawke, L. G. D.; Huang, Q.; Hassager, O.; Read, D. J. Modifying the pom-pom model for extensional viscosity overshoots. *J. Rheol.* **2015**, *59*, 995−1017.

(44) Ianniruberto, G. Quantitative appraisal of a new CCR model for entangled linear polymers. *J. Rheol.* **2015**, *59*, 211.

(45) McIlroy, C.; Olmsted, P. D. Deformation of an amorphous polymer during the fused-filament-fabrication method for additive manufacturing. *J. Rheol.* **2017**, *61*, 379.

(46) Teng, C.; Gao, Y.; Wang, X.; Jiang, W.; Zhang, C.; Wang, R.; Zhou, D.; Xue, G. Reentanglement Kinetics of Freeze-Dried Polymers above the Glass Transition Temperature. *Macromolecules* **2012**, *45*, 6648−6651.

(47) Shchetnikava, V.; Slot, J. J. M.; van Ruymbeke, E. A comparison of tube model predictions of the linear viscoelastic behavior of symmetric star polymer melts. *Macromolecules* **2014**, *47*, 3350−3361.

(48) Hawke, L. G. D.; Ahmadi, M.; Goldansaz, H.; van Ruymbeke, E. Viscoelastic properties of linear associating poly(n-butyl acrylate) chains. *J. Rheol.* **2016**, *60*, 297−310.

(49) Robertson, C. G.; Warren, S.; Plazek, D. J.; Roland, C. M. Reentanglement Kinetics in Sheared Polybutadiene Solutions. *Macromolecules* **2004**, *37*, 10018−10022.

(50) Roy, D.; Roland, C. M. Reentanglement Kinetics in Polyisobutylene. *Macromolecules* **2013**, *46*, 9403−9408.

(51) Andablo-Reyes, E. A.; de Boer, E. L.; Rastogi, S.; Rastogi, S. Stress relaxation in the nonequilibrium state of a polymer melt. *J. Rheol.* **2014**, *58*, 1981−1991.

DOI: 10.1021/acs.macromol.9b01152